INEEL/EXT-99-00693
MIT-ANP-TR-065
July 1999

Advanced Reactor Technology

Design of an Actinide Burning, Lead-Bismuth Cooled Reactor That Produces Low Cost Electricity

Annual Project Status Report
June 1999

Principal Investigators

Jacopo Buongiorno MIT-Reactor Design
Ron Ballinger MIT-Material Studies
Cliff Davis INEEL-Reactor Design
Kim Doyoung MIT-Materials
Mikael Driscoll MIT-Neutronics
Pavel Hejzler MIT-Neutronics
Steve Herring INEEL-Neutronics
Mujid Kazimi MIT-Reactor Design
Philip MacDonald INEEL*-Fuel Design and Material Studies
Kathy McCarthy INEEL-Materials Studies
Neil Todreas MIT*-Reactor Design
Vik Shah INEEL-Materials Studies
Kevan Weaver INEEL-Neutronics

*** Project Leadership**

DISCLAIMER

DISCLAIMER

Portions of this document may be illegible in electronic image products. Images are produced from the best available original document.

TABLE OF CONTENTS

1. Project Overview

The purpose of this project is to investigate the suitability of lead-bismuth cooled fast reactors for producing low-cost electricity as well as for actinide burning. The goal is to identify and analyze the key technical issues in core neutronics, materials, thermal-hydraulics, fuels, and economics associated with the development of this reactor concept.

While considerable design work has been done in the United States, Europe, and Japan on fast reactors, including actinide burners, it has mostly been done for sodium cooled reactors. A lead-bismuth cooled fast reactor was considered in the United States in the 1950s. However, it was abandoned in favor of sodium cooling for two reasons: (1) lead bismuth coolant at the temperatures of interest can be very corrosive to structural materials; and (2) the doubling time of sodium cooled fast reactors can be significantly shorter than that of lead-bismuth cooled reactors as a result of the higher power density achievable in sodium cooled cores. Whereas a short doubling time was considered an important performance characteristic in the fifties, it is of little significance today, as we do not foresee a depletion of low cost uranium resources in the near future, and we have a significant inventory of actinides which can be burned in a fast reactor. Regarding the material compatibility issue, the Russians adopted lead-bismuth for use in their most advanced nuclear submarines, the so-called "Alpha" class submarines which are the fastest in the world. The Russians have built and operated seven Pb-Bi reactors in submarines and two on-shore prototypes. More recently they have studied the design of a variety of lead and lead-bismuth reactors for electric power generation, some of which can operate with one core loading for many years and do not require any fuel reprocessing. Elsewhere, very long-lived core, lead-bismuth cooled, fast reactors have been investigated in Japan, and in the US at the University of California at Berkeley. A lead-bismuth cooled, accelerator-driven, sub-critical actinide burner has been proposed by the Los Alamos National Laboratory for burning the actinides and long-life fission products from spent light water reactor fuel. The Los Alamos system has been labeled Accelerator-driven Transmutation of Waste (ATW). It is envisioned that the reactors investigated in this study could operate in concert with ATWs in a program to both burn the waste from the current generation of light water reactors and produce low-cost electricity. It should also be noted that there exists a synergy between the development of the ATW and a critical system: they share similar coolant and fuel technologies with the result that either system can greatly benefit from improvements achieved for the other.

The choice of lead-bismuth for the reactor coolant in an actinide burning fast reactor offers enhanced safety and reliability. The advantages of lead-bismuth over sodium as a coolant are related to the following material characteristics: chemical inertness with air and water; higher atomic number; lower vapor pressure at operating temperatures; and higher boiling temperature. These basic properties lead to the following advantages for lead-bismuth coolant:

- harder neutron spectrum and, therefore, improved neutron economy, especially when burning actinides;

- better reflection properties, therefore, it is possible to get breeding even without blankets;
- better shielding against gamma-rays and energetic neutrons;
- practically impossible to create a major void in the core due to coolant overheating due to the high boiling temperature and high heat of vaporization of lead-bismuth (a boiling temperature of 1725 C versus 892 C for sodium);
- possibility of eliminating the intermediate coolant loop, and reducing capital costs;
- possibility of using high efficiency heat transfer cycles;
- simpler containment structure due to the impossibility of fires and explosions; and
- small volume change upon solidification.

There are disadvantages to the use of lead-bismuth for cooling an actinide fast reactor in addition to the material compatibility problems. These include: high material cost; higher melting temperature (125 versus 98°C); and the production of Po-210.

Given the status of the field, it was agreed that the focus of this investigation in the first two years will be on the assessment of approaches to optimize core and plant arrangements in order to provide maximum safety and economic potential in this type of reactor. It is envisioned that one pool type plant design would be explored that could accommodate two cores (1) a long-lived core utilizing fertile metal fuel that will consume actinides and (2) a core utilizing non-fertile metal fuel which will maximize the actinide consumption. INEEL and MIT will both work on the plant design. For the first year MIT will focus on the non-fertile fueled core while INEEL will focus on the fertile long-lived core. Four disciplinary-based areas are to be initially investigated:

Neutronic Core Design. Using MOCUP, which combines the MCNP and ORIGIN codes, both MIT and INEEL will investigate the optimum loading of actinides and other materials to create a core that has suitably negative Doppler and void coefficients and a suitably long reactivity lifetime. The work at MIT will initially focus on the use of non-fertile metal fuel. The INEEL will investigate both non-fertile and fertile metal and nitride fuels, looking for optimum economics for an actinide burning, low cost of electricity, reactor design.

Thermal-hydraulic Design Optimization. MIT will investigate pool-type plant designs that will achieve maximum natural convection capability for the core, with the goal of achieving full power removal by natural circulation. MIT will also investigate the economic and safety potential for using a gas turbine power conversion cycle. INEEL will assess the economic and safety potential of the pool type reactor using a steam cycle. INEEL will also assess the plant transient response to various initiating accidents using a modified version of RELAP to account for the coolant and neutronic characteristics.

Fuel and Material Studies. MIT will investigate the suitability of materials for operation over a range of core exit temperatures that will result in economic operation with a secondary side gas cycle. INEEL will investigate the advantages and tradeoffs among various fuel materials such as zirconium-based metallic fuel, oxide fuel and nitride fuel.

Chemical Separation and Waste Assessment. Depending on the fuel materials selected, MIT will perform an assessment of separation technologies and waste disposal strategies in year two.

2. KEY TECHNICAL CHALLENGES

Several technical challenges have been identified that are peculiar to this reactor design.

2.1 Neutronics

Several different fuel types can be used depending on the scope and purpose of the reactor. These fuel types can be lumped into two general categories: fertile and non-fertile fuels. Each type has its own set of challenges, although some of the problems are common to both. The group at MIT has focused on evaluating the behavior of non-fertile fuel, while the group at the INEEL has focused on evaluating the behavior of fertile fuels in a lead-bismuth cooled fast reactor.

To effectively transmute plutonium and minor actinides from LWR spent fuel, it is desirable to minimize the waste of neutrons in order to attain a large surplus available for transmutation. Metallic fuels based on a zirconium matrix provide large excess reactivity due to the low parasitic absorption cross-section of zirconium and due to the hard spectrum achievable because the fuel does not contain any moderating isotope. Nitride fuels may also be suitable.

To maximize the *actinide transmutation* capability of the system, breeding of new fissile material must be minimized hence making the presence of the fertile isotopes U-238 or Th-232 undesirable. The choice of fuel composition for maximum actinide transmutation is then restrained to the to-be-transmuted plutonium and minor actinides (20-30% wt.) and to the zirconium matrix (70-80% wt.), constituting the structural component of the fuel rods. It should be noted that the larger weight fraction of zirconium relative to the heavy metals makes this non-fertile fuel significantly different from the metallic fuel developed by ANL for the IFR project. We envision using dispersion type fuel with IFR type coated particles dispersed in a pure zirconium matrix.

However, to minimize the *cost of electricity* produced, it is desirable to have relatively long refueling cycles so that the plant capacity factors are high and the fuel fabrication costs are low. Long refueling cycles require relatively constant reactivity and, therefore, the use of some fertile material in the fuel. Thorium, with enough depleted uranium to dilute the U-233, is the material of choice, because the end product is not easily separable. Again, a dispersion type metallic fuel with coated plutonium-thorium-uranium particles in a zirconium matrix is envisioned.

The choice of a non-fertile metallic fuel raises three major neutronic challenges:

a) large positive coolant void reactivity coefficient,
b) small Doppler feedback,
c) large rate of reactivity loss with burnup (i.e. the so-called reactivity swing).

In a fertile system, the choice of fuel composition does include the fertile isotopes U-238 or Th-232 (or both), while retaining the to-be-transmuted plutonium and minor actinides present in the non-fertile fuel as the fissile component. The challenge with the fertile fuel is the positive coolant void reactivity coefficient.

Void Reactivity Coefficient. The sign of the coolant void coefficient in fast reactors is the combined result of three conflicting effects upon coolant voiding:

- neutron leakage is increased resulting in reactivity reduction,
- neutron scattering decreases and the spectrum hardens resulting in larger fission-to-capture ratio hence increasing reactivity,
- parasitic captures in the coolant decrease leading to a reactivity increase.

The net outcome is typically a strong reactivity increase due to the latter two effects unless leakage is enhanced enough to offset them.

Doppler Reactivity Coefficient. The amount of fertile isotopes in the non-fertile metallic fuel is very small (mostly Pu-240). Moreover, the hard spectrum leads to a decrease of absorption rate in the resonance peaks. Both these factors result in a very small Doppler feedback and measures to attain a reasonably negative Doppler coefficient must be employed for non-fertile fuel. The fertile fuel can overcome this problem by including enough fertile material to attain a reasonably negative Doppler coefficient.

Reactivity Swing with Burnup. A major consequence of the absence of fertile isotopes is the faster net depletion of the fissionable material and hence a marked reduction of reactivity during a cycle. To ensure criticality at EOL, the reactivity excess at BOL must be large, making this design potentially vulnerable to accidents related to malfunction of the control rod mechanisms (e.g. rapid control rod ejection). In the fertile fuel, the reactivity swing should be very small, requiring less excess reactivity. However, for long-lived fuel the excess reactivity must be sufficient to sustain criticality throughout the life of the reactor.

These challenges are common to most fast reactors and their magnitude is illustrated in **Table 1** for the ANL sodium-cooled, metal-fueled Integrated Fast Reactor (IFR) and for three different fuel compositions.

Table 1. Reactivity swing, void worth, and doppler coefficients in sodium cooled, metal fueled fast reactors.

	Traditional Breeder Fuel	**Fertile-free fuel**	
Parameter		Weapon Grade Pu Fuel[1]	LWR TRU Fuel[1]
Reactivity Swing ($)	0.09	15.8	7.8
Na void worth ($)	4.78	19.8	6.51
Doppler (¢/K)	-0.05	-0.01	-0.07

2.2 Plant Engineering

2.2.1 Primary System Cost: Enhanced Natural Circulation and Passive Decay Heat Removal System

Key technical objectives are to simplify the primary system, improve its overall reliability and make operation and maintenance less expensive. The development of a passive Decay Heat Removal System (DHRS) and a primary coolant system with enhanced natural circulation capability are potential means to achieve these objectives.

Two options have been considered relative to enhancing natural circulation. One option uses pumps to produce forced convection through the primary coolant system during normal operation, but relies on natural circulation when the reactor is shutdown and just the decay heat is to be removed. The second option relies exclusively on natural circulation in the Pb-Bi, even at full power.

To achieve full power natural circulation in the second option, it may be necessary to design the primary system to allow a substantial relative elevation (i.e. the so-called gravitational head) between the core and the heat sink. Also, friction and form pressure losses must be minimized everywhere in the primary system. These requirements may be in conflict with the need to keep the size of the system within reasonable limits and with the neutronic constraints on the fuel lattice openness[2]. Moreover, a large primary system implies a large inventory of bismuth, which is a relatively costly material.

A shorter reactor pool can be designed if the goal of natural circulation is pursued by mixing the primary coolant with an inert gas[3] in the hot leg to attain a large driving density difference as proposed by Branover [1988]. However, it should be noted that a minimum inventory of primary coolant is required to ensure a sufficient thermal inertia of the reactor pool, which is necessary to smooth transients and to mitigate the consequences of loss of normal heat sink accidents. In this respect it is particularly important to ensure

[1] Fuel with Hf addition to augment the doppler feedback.
[2] A loose lattice may not be neutronically acceptable because it increases the capture in the coolant and worsens the void reactivity feedback.
[3] This is the so-called gas-pump approach.

that enough decay heat can be accumulated in the reactor pool without excessive temperature rise before the DHRS comes online to provide a long-term heat sink.

The low chemical reactivity of Pb-Bi with water and air eliminates the need for the costly intermediate loop typical of sodium cooled fast reactors. However, placing the primary-to-secondary heat exchanger directly in the reactor pool raises a new kind of concern regarding the reactivity response to core flooding by the secondary coolant (i.e. water or helium) in case of heat exchanger tube failure. Thus, the primary coolant flow path in the reactor pool may have to be designed to prevent entrainment of undesirable fluids in the core.

It is clear then that selecting the primary system configuration is an involved challenge driven by the trade-off between forced and natural circulation, neutronics, safety, cost and decay heat removal requirements.

2.2.2 Operating Costs: High Efficiency Power Cycle and Materials Corrosion Control

It is essential to maximize the production of electricity in order to improve the economic acceptability of the system. A suitable conversion power cycle to best exploit the thermal power produced in the core is to be selected: both gas and steam turbine power cycles are potential candidates.

Gas turbine cycles are simpler, easier to operate and, if a chemically inert gas is selected as the working fluid (e.g. helium), they do not pose any major corrosion problems. However, they may have to be operated at high temperature (>550°C) to attain an acceptable thermal efficiency. Moreover, it should be noted that the operating experience with helium turbines is limited.

On the other hand the use of a steam cycle ensures thermal efficiencies above 30% at relatively low temperatures (<350°C), as proven in LWR plants.

In any case a high Pb-Bi temperature in the primary system is desirable since it increases the thermal efficiency of the power cycle. Given the corrosive nature of liquid lead-bismuth at high temperature, the development and selection of compatible structural materials becomes a key issue. Normal austenitic stainless steels cannot be used because nickel rapidly dissolves in bismuth. Current materials investigations focus on the characteristics of a martensitic-ferritic stainless steel (designated EP-823) of low nickel and high silicon content especially developed in Russia for Pb-Bi applications. Moreover, the extremely hard neutron spectrum raises additional concerns regarding the mechanical performance of the reactor materials: the permanent supporting structures in the core (e.g. the core plate, the core barrel) are expected to be irradiated at neutron fluences that may cause significant swelling and embrittlement.

Finally, special emphasis is given to the theoretical determination of the thermo-physical and mechanical properties of the selected fuel because very little data relevant to

this fuel are available in the literature. Nevertheless it should be noted that a fuel mainly composed of Zr (as opposed to a fuel mainly composed of actinides, like the IFR fuel developed by ANL) is expected to yield better overall performance due to the larger thermal conductivity, the superior physical stability (i.e. less changes of phase) and mechanical characteristics of Zr compared to actinides. A coated particle dispersion type of arrangement may further improve the performance of this fuel.

2.2.3 Coolant Activation

The long-lived α-emitter ^{210}Po is produced in the coolant by the following nuclear reaction:

$$^{209}Bi + n \rightarrow {}^{210}Bi \underset{t_{1/2}=5days}{\overset{\beta^-}{\rightarrow}} {}^{210}Po$$

Preliminary calculations show that the concentration of this radionuclide in the primary coolant can reach several hundreds of Ci per liter of Pb-Bi if not continuously removed by means of an active purification system. Given the high radio-toxicity of this nuclide, its Derived Air Concentration (DAC) limit is very stringent (10 Bq/m^3) and special attention must be paid to ensure that the releases of contaminated Pb-Bi are minimized.

2.2.4 System Analysis Capability

One technical challenge is to develop a thermal-hydraulic system analysis capability that can be used in both the design of the reactor and in the evaluation of its safety. The system analysis capability allows for a simultaneous modeling of the primary and secondary coolant systems, the decay heat removal system, and the reactor neutronics at normal operation and during transients and accounts for the interactions between systems. The approach taken to meet this challenge is to modify an existing thermal-hydraulic system analysis code, based on RELAP5 (LMITCO 1995), to represent a Pb-Bi reactor.

3. Design Progress

This section presents the design results that have been achieved since project inception in October 1998. These design results derive from the effort that has been aimed at exploring and surmounting the design challenges presented in Section **2**.

3.1 Neutronics (MIT)

3.1.1 Void Reactivity Coefficient in a Non-fertile, Metal Fuel Core

A major effort was focused on the development of a non-fertile, metal fuel core with a negative reactivity coefficient when the whole core is voided, or when only a limited region of the core is voided. The latter situation may arise if a steam generator tube ruptures and a subsequent steam or helium bubble is transported into the core, or in the case of cladding failure and gas release from one or more fuel rods. Pursuing the goal of reactivity decrease upon partial core voiding will add complexity to the fuel assembly design; therefore, a detailed analysis of various accident situations must ultimately be undertaken to assess if a negative partial void reactivity coefficient is really necessary.

Several strategies to attain negative void coefficient were explored by means of the MCNP code. They involve:

- Decreasing the pitch to diameter ratio to reduce the magnitude of the positive void coefficient due to smaller change of absorption rate in coolant and smaller spectrum shift from coolant voiding. However, the reduction of pitch to diameter was restricted because of thermo-hydraulics limitations and even tight pitch to diameters were not able to achieve negative coolant density coefficient.
- Loading the ends of fuel pins with stainless steel reflector material followed by B_4C absorber pellets enriched with B^{10} or zirconium hydride to increase leakage/absorption to peripheral absorbers upon coolant voiding. This approach enabled the attainment of negative reactivity change with coolant density. However the drawback was a more complicated fuel rod design and an appreciable reactivity penalty.
- Reducing core height to increase leakage in the axial direction. Core heights of about 1m yielded a negative reactivity change with coolant density.
- Introducing blanket assemblies heterogeneously placed in the core to increase leakage into these blankets upon coolant voiding.

Although the pin shields with absorbing material, pancake cores with small height, or heterogeneous cores with blanket assemblies provided negative reactivity change with decreasing coolant density*, none of these strategies appeared to be effective when only the central region of the core was voided. Therefore, an effort has been made to design a

* Reactivity changes were calculated by varying the core-average coolant density, which was assumed uniform over the entire core, while coolant in the lower-plenum, in the radial reflector and in the chimney above the core were kept constant.

core that can avoid reactivity spikes in the event of partial core voiding. This can be done if neutrons can leak directly from the core center.

Two approaches were found to be effective. The first design involves a pressure-tube reactor similar to the CANDU design with gas-filled space between the pressure tubes. However, pressure tubes pose significant material problems in a high-flux fast reactor with a hard spectrum. Also inadvertent flooding of the inter-tube space with coolant from failed pressure tubes results in a reactivity increase. Therefore, the design of a fuel assembly that allows streaming of neutrons in both radial and axial directions from the center of the core was considered. A number of various streaming fuel assemblies and core configurations have been investigated. One of the alternatives giving plausible void reactivity performance is shown in **Figure 1**.

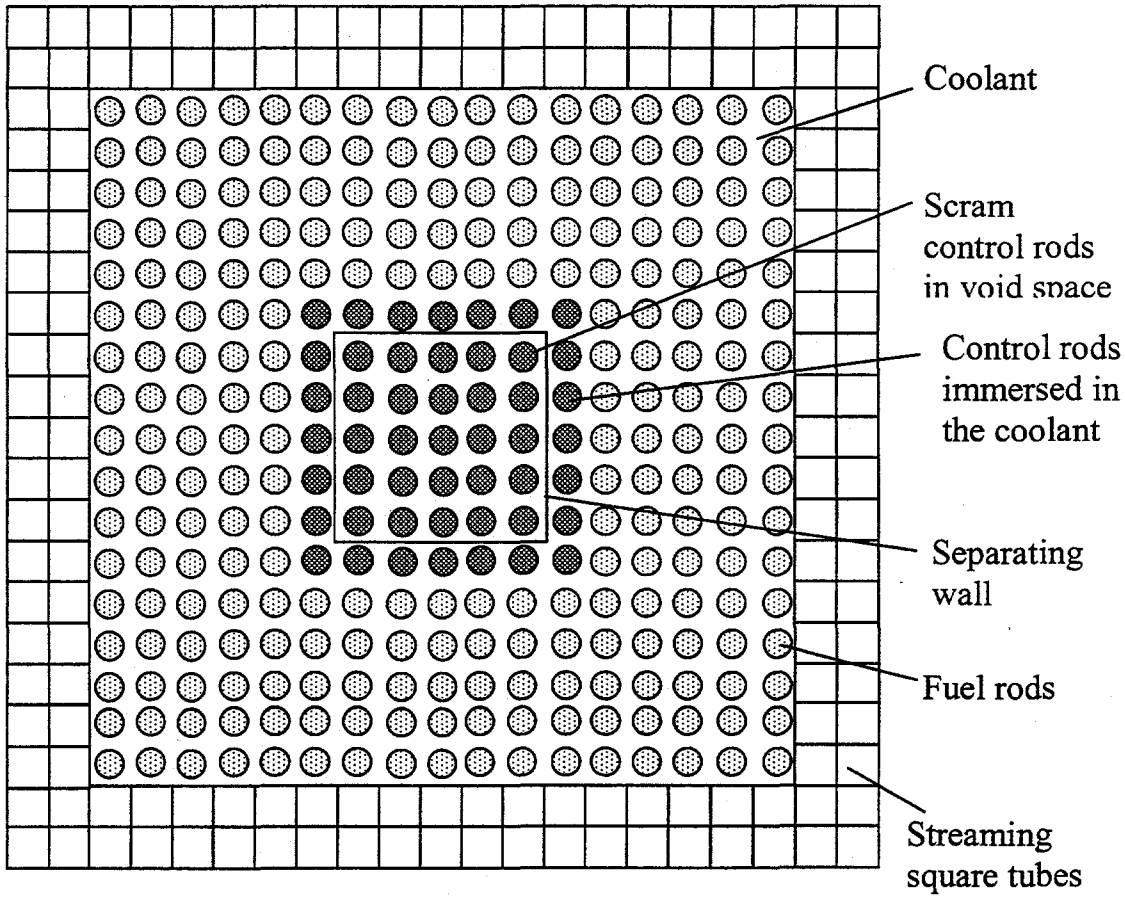

Figure 1 Schematic of fuel assembly with control rod drives

The assembly contains 21×21 positions with 240 fuel rods, 152 square streaming tubes arranged in two rows at the fuel assembly periphery and 7×7 positions in the fuel assembly center. The streaming tubes are filled with gas and sealed. In addition to their neutron streaming function, they also provide structural support for the assembly making possible elimination of separate tie rods. In case of failure of a streaming tube, only one

tube will be flooded with coolant leading to a very small reactivity increase. To achieve a significant reactivity change in such a scenario, a very large number of these tubes would have to be simultaneously flooded. Widespread void flooding is thus extremely unlikely. The thickness of the walls of the square tubes was taken the same as that of cladding, i.e., 0.63mm. The central region of each fuel assembly contains a 5×5 void space to enhance neutron streaming. This space is also used for scram control rods (located outside the core under normal operating conditions). An additional 24 control rods are located around the assembly central region to compensate for long term reactivity decrease and to control the reactor power in transients (for a more comprehensive discussion on the control system see Section 3.4.5).

The core schematic in **Figure 2** shows the location of the fuel rods within the assemblies and the relative power in each fuel assembly. The control rods are made of B_4C with 90% B10 enrichment and are used for both reactivity compensation and control. The main data used for neutronic analysis are summarized in **Table 2**.

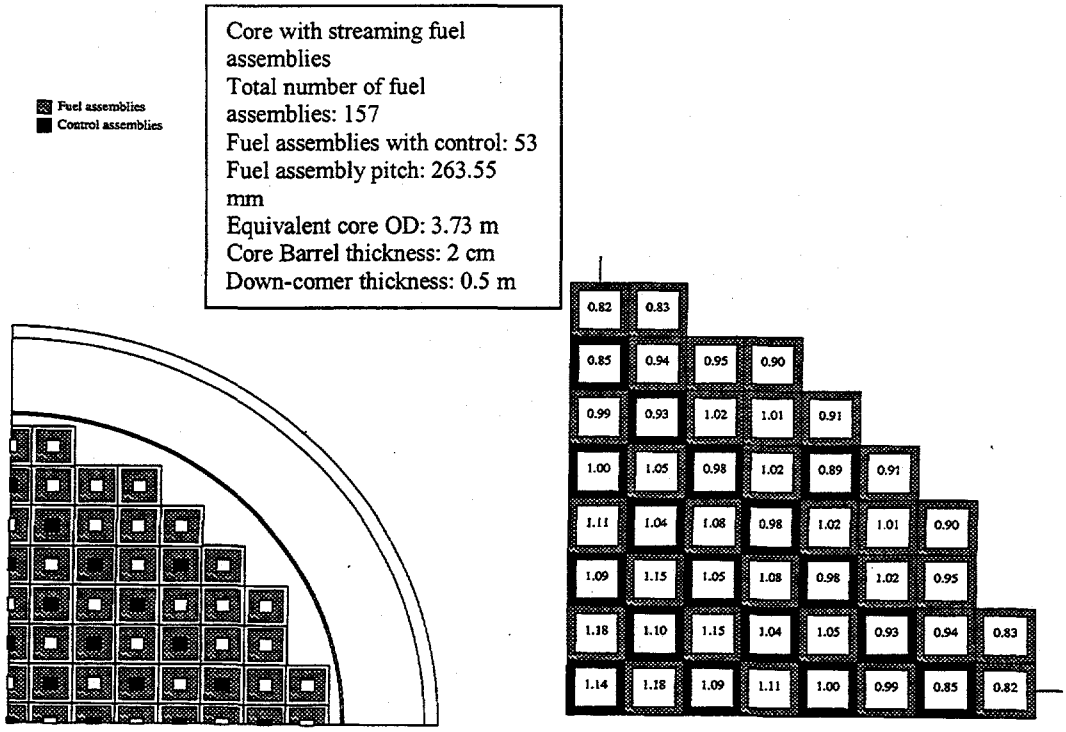

Figure 2 Core layout and fuel assembly power distribution

Table 2 also gives the effective multiplication coefficients for various states of the core. Reactivity exhibits a decreasing trend with decreasing coolant density. Partial core voiding also yields a reactivity decrease, both in case of voiding 50% of 4 fuel assemblies or in case of 50% voiding of only one central fuel assembly. At high burnups, the void reactivity behavior gets slightly worse, as the fuel composition changes to a less favorable state with respect to variation of capture and fission cross sections due to spectrum hardening. However, the reactivity increase at high burnup for the case of partial voiding of 4 fuel assemblies is very small. The calculations also show that flooding either the

entire bank of fuel assembly peripheral streaming tubes (152 tubes) or of the fuel assembly central void region results in reactivity reduction. Hence, the core design with streaming fuel assemblies appears very promising and apparently overcomes the void reactivity problem.

Table 2. Reactivity performance of the fresh core (uniform enrichment)

Case (control rod drives are 84.5cm in the core unless specified otherwise)	k_{eff}
Reference case (core-average coolant density =10.25g/cm^3)	0.999±0.001
Core-average coolant density =8g/cm^3	0.992±0.001
Core-average coolant density =6g/cm^3	0.988±0.001
4 fuel assemblies voided*	0.998±0.001
Control rod drives from the central fuel assembly fully withdrawn	1.004±0.001
Worth of central control assembly	0.005k/k
1 central fuel assembly voided** (for fully withdrawn control rod drives in central fuel assembly)	1.002±0.001
1 central fuel assembly fully flooded –all peripherial streaming tubes (152) flooded	0.996±0.001
Entire central void region with control rod drives 84.5cm in the core in central fuel assembly flooded	0.998±0.001
All control rod drives fully withdrawn - burnup=0GWd/tHM –coolant density=10.25g/cm^3	1.241±0.001
All control rod drives fully withdrawn - burnup=198GWd/tHM+-coolant density=10.25g/cm^3	1.031±0.001
All control rod drives fully withdrawn - burnup=198GWd/tHM+- 4 fuel assemblies voided*	1.032±0.001
All control rod drives fully withdrawn - burnup=198GWd/tHM+-coolant density=8g/cm^3	1.031±0.001

* Partially voided central 50% of 4 fuel assemblies in the core central region

** Partially voided central 50% of 1 central fuel assembly (control rod drives from this assembly withdrawn)

+ 198 GWd corresponds to 632 full power days of exposure, tHM is metric tons of heavy metal

The large reactivity compensation by the control rods results in a relatively large axial power peaking at BOL, as shown on **Figure 3**. Modifications of the control system will be introduced in this effort to lower this peaking.

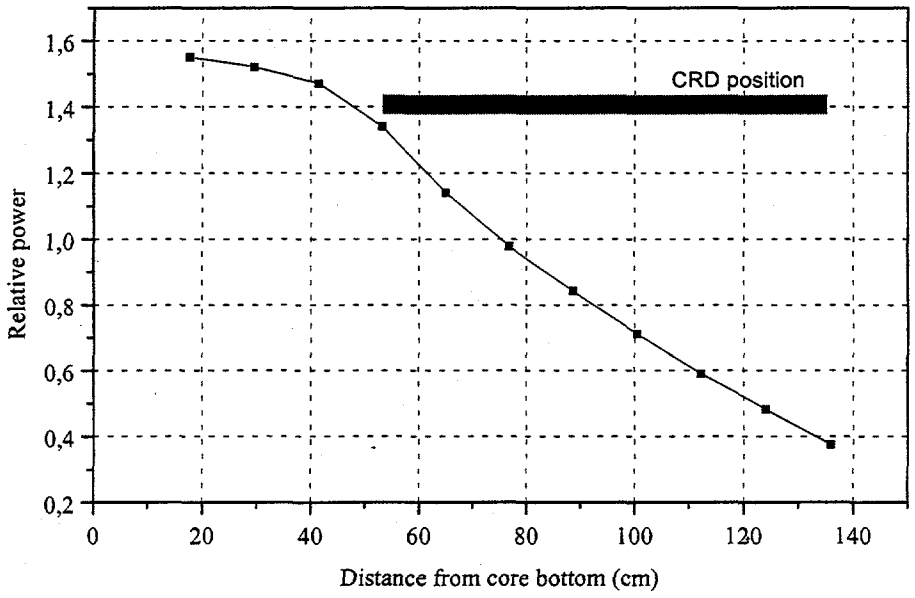

Figure 3 Axial power density profile (average over all fuel rods) at BOL

3.1.2 Reactivity Changes with Burnup and TRU Consumption Rate in a Non-fertile, Metal fuel Core

Changes of fuel compositions during burnup were modeled using MOCUP using a unit cell model. The fuel composition obtained from this unit-cell model at selected burnups was then used in the full core model to obtain k_{eff}. The results are plotted in **Figure 4**.

It can be observed that the core can operate for about 1.7 years, achieving burnup of 190,000MWd/t of heavy metal. Several burnable absorber materials, such as Re, B-10 or Sm-149 were placed in the zirconium matrix and were evaluated to explore options of reducing the slope of the burnup curve as a means to reduce rod worth and extend cycle length. Boron exhibited the best performance, but none of the isotopes investigated appeared very effective. Although the slope of the reactivity slope was reduced, the burnup rate of the absorbers was low due to their small cross section in a hard spectrum yielding a large residual inventory at end of life. Since no materials were identified with significantly larger capture cross sections than those of boron, burnable poisons were discarded in favor of excess reactivity compensation through control rods.

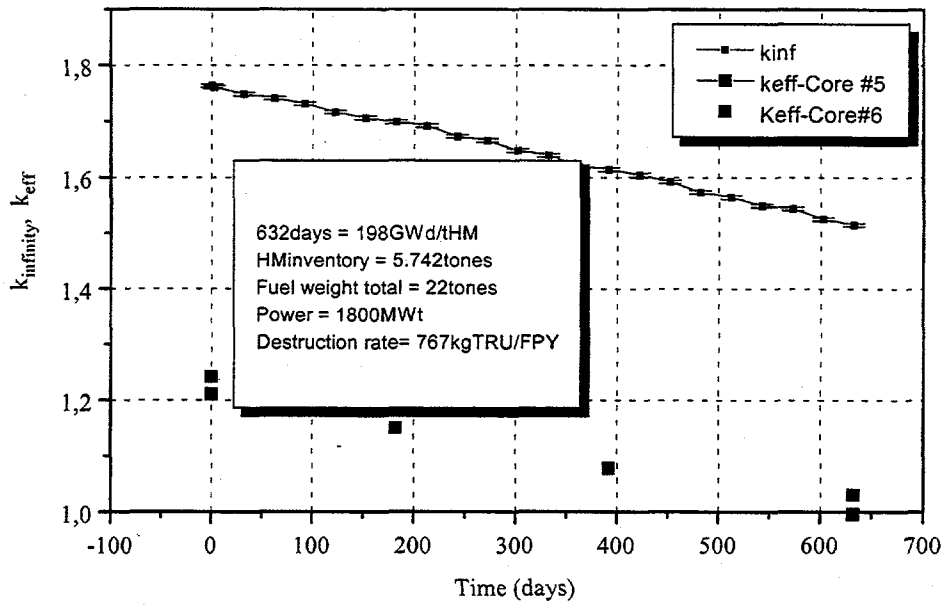

Figure 4. Reactivity change with burnup

The destruction rate of individual actinides per full power year, as obtained from MOCUP, is plotted in **Figure 5**. These results indicate that the proposed Pb-Bi burner with streaming fuel assemblies is quite effective for actinide burning. The total destruction rate of TRUs at an operating power of 1800 MWth is about 767 kg/FPY. This compares with 650 kg/y per 2000 MWth for ATW [Venneri 1998], or 585 kg/y per 1800 MWth. However, this comparison does not include the capacity factor of ATW, which was not known to us. If an ATW capacity factor of 0.8 was assumed, the ATW destruction rate would be 731 kg/FPY. The spallation reactions deposit appreciable heat within the system, hence for the fixed total thermal power, the fission-generated power output, which is the key factor for the incineration rate, is smaller than in the case of a Pb-Bi critical burner. Consequently, the ATW destruction rate is less, which should explain the difference between the values of 767 and 731 kg/FPY above. Hill et al., [1995] studied a sodium cooled fast reactor as a pure burner using metallic fuel and estimated a destruction rate of 231 kg TRU/y per 840 MWth at a capacity factor of 0.75. Scaling their power to 1800 MWth and incorporating the capacity factor yields a destruction rate of 660 kg TRU/FPY. Since the power released per fission is approximately the same for Pb-Bi and sodium-cooled fast reactors, the number of fissions is also comparable for the fixed core power. Therefore, the reason for different TRU consumption rate must come

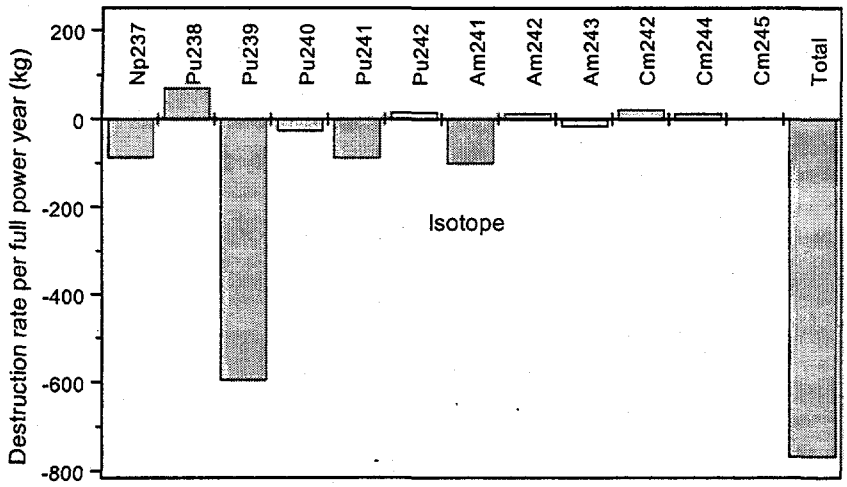

Figure 5. Destruction rate per full power year of various isotopes calculated by MOCUP for a non-fertile, metal fuel core.

from spectral effects. The very hard spectrum of the Pb-Bi burner results in less captures and therefore a smaller conversion ratio. For example, for the given core design, the conversion ratio* is only 0.23. Consequently, the net effect is a higher destruction rate of actinides.

3.2 Neutronics (INEEL)

3.2.1 Comparison of Reactivity Swings with Information Published by Sekimoto

Japanese researchers (Sekimoto and Su'ud) at the Tokyo Institute of Technology have performed a 2-dimensional analysis of possible lead and lead-bismuth reactors using the SLAROM computer code. In their first analysis, they constructed a block core that contained a shield, reflector, outer core, middle core, and central core. A modification, which included blanket material within the central and middle core region, was also analyzed. The fuels used in the calculations were metallic (10% Zr) and nitride, with the nitride fuel slightly outperforming the metallic fuel. Also included in the calculations were different fuel enrichments using plutonium as the fissile component, and a fuel volume percent of 45-50%. The coolants studied were lead and lead-bismuth, with lead-bismuth showing better overall properties. The calculations were performed for a core

---

* Conversion ratio is defined here as $CR = \sum \sigma_{c,j} N_j \phi / \left(\sum \sigma_{c,j} N_j \phi + \sum \sigma_{f,j} N_j \phi \right)$, where the sums are over all heavy metal nuclides, j.

lifetime that was to exceed 10 years without refueling or fuel shuffling, while maintaining burnup reactivity swings to less than 0.1% Δk/k. Other restrictions include maintaining a negative total-core coolant void coefficient of reactivity over all of the burnup period, omission of an intermediate heat exchanger, and a large natural circulation contribution. Their 2-dimensional calculations show that a reactor can maintain criticality for ~12 years with the above limitations.

This block core was used as a reactivity benchmark to compare a 3-dimensional analysis with a 2-dimensional one. This was accomplished by using MOCUP to perform a time-dependent treatment of nuclides within the reactor. The core was modeled using homogenous fuel blocks, with the pin shields and reflectors also being modeled as homogenous blocks. The burnup steps were performed at one-year intervals for a total burnup of 12 years. Thus far, three cores have been burned using different fuel volume percentages. The Sekimoto results can be seen in **Figure 6**, and the MOCUP results are summarized in **Figure 7**. Sekimoto's results show a decrease in reactivity during the first 3 years, and then an increase between the third and fourth year, with a peak occurring between the eighth and ninth years. He attributes this reactivity swing to the buildup of fissile plutonium from the fertile U-238 in the fuel. This is notably different from the reactivity swing found in the MOCUP results. The slope of the reactivity change with time in all three MOCUP cases is almost identical; there is no gradual increase in the reactivity. By extrapolation, an optimum fuel volume percentage for a 12-year burn can be found at ~46%. This is within the same volume percent range that Sekimoto used to achieve a 12-year critical cycle.

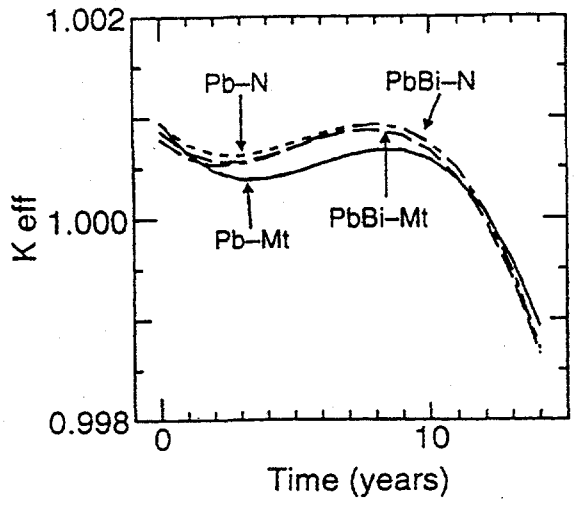

Figure 6. Reactivity of Sekimoto core using different fuels and coolants.

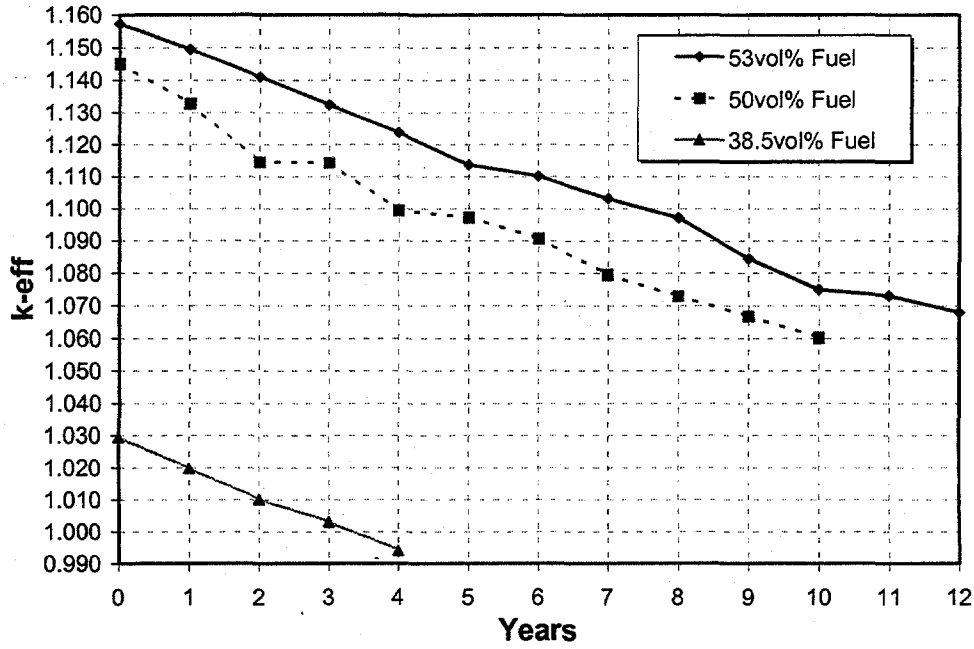

Figure 7. MOCUP calculated reactivity changes with time in the Sekimoto core for three fuel types: 38.5, 50, and 53 volume percent fuel.

3.2.2 Evaluation of Fertile Fuel Options

The advantages of using fertile fuel compared to a non-fertile fuel are:

- better Doppler reactivity coefficient,
- smaller reactivity swing throughout the life of the reactor, and
- longer fuel life.

While these advantages can be significant over a non-fertile system, there still remains the problem of the coolant void coefficient, and the rate at which the actinides can be burned compared to a non-fertile fuel. The void coefficient was addressed in a previous section and will not be re-addressed here. The TRU consumption rate for a fertile fuel will depend upon the reactor power, the TRU content, and the economics involved. The economics will be addressed later.

Because one of the goals of this reactor is to burn actinides, the composition of a fertile fuel must be carefully chosen so as not to produce more actinides than are to be burned, yet the reactor must still be capable of long refueling cycles. This particular requirement would seem to favor thorium over uranium as a fertile material, especially if nonproliferation by way of plutonium production in the reactor is considered an important factor. However, the production of U-233 from thorium must also be considered as a proliferation concern, which would necessitate the addition of some uranium to the fuel (preferably depleted uranium). With these considerations in mind, unit-cell calculations using MOCUP were performed on metallic and nitride fuels. The plutonium and minor actinide composition was held constant at 20% wt., with the

remainder being either uranium/zirconium or thorium/zirconium, and only zirconium in the case of the non-fertile fuel. **Table 3** gives a summary of the fuel composition at BOL.

Table 3. Fertile and non-fertile fuel composition (BOL).

	Non-fertile (wt%)	**Metallic** (wt%)	**Nitride** (wt%)
Plutonium	**16%**	**16%**	**16%**
Pu-238	0.32%	0.32%	0.32%
Pu-239	9.28%	9.28%	9.28%
Pu-240	4.16%	4.16%	4.16%
Pu-241	1.6%	1.6%	1.6%
Pu-242	0.64%	0.64%	0.64%
Minor Actinide	**4%**	**4%**	**4%**
Np-237	1.72%	1.72%	1.72%
Am-241	1.8%	1.8%	1.8%
Am-243	0.36%	0.36%	0.36%
Cm-244	0.12%	0.12%	0.12%
Uranium (nat.) – if used	-	**70%**	**74.5%**
Thorium – if used	-	**70%**	**74.4%**
Zirconium	**80%**	**10%**	-
Nitrogen	-	-	**5.5%** (w/ U) **5.6%** (w/ Th)

The next consideration in using these different fuel types is the reactor power level. This issue becomes important for long-lived cores because the amount of fissile material that will be needed to sustain a critical reactor will have to be adjusted or optimized. The fissile components used for the current analysis are Pu-239 and Pu-241, and were kept constant at a combined weight percent of 10.88%. Although choosing a constant weight percent means that the atom densities for the fissile plutonium will be different for each case, the results of the calculations will be used to extrapolate to an optimal fuel composition. The power levels were chosen at 833 MWth (300 MWe) and 5000 MWth (1800 MWe) with more calculations to be done at 2777 MWth (1000 MWe). The calculations assumed an efficiency of 36%.

The current analysis has been limited to IFR type fuel, i.e., cylindrical pins placed in assemblies. The parameters of the pin can be seen in **Table 4**. The metallic fuel has two interesting properties that are unique to this type of fuel:

- The gas plenum above the fuel.
- The materials used in the gap between the fuel and the cladding.

The gas plenum is used to capture the fission gases as they diffuse from the metallic fuel. This plenum may be reduced somewhat if a dispersion fuel is used in place of the IFR type fuel. The gap material is used to enhance the thermal conductivity of the fuel. However, use of a dispersion fuel would probably eliminate the need for gap materials. It is important to note that other fuel geometries may show better neutronic or thermal hydraulic properties, and will be studied once the fuel composition has been optimized.

Table 4. Parameters of the cylindrical fuel pins.

Design Parameter	**Value**
Fuel OD	0.864 cm
Gap Thickness	0.02 cm
Gap Material (metallic fuel only)	33wt% Pb - 33wt% Sn - 33wt%Bi
Cladding Thickness	0.063cm
Cladding OD	1.03 cm
P/D	1.6
Active Fuel Height	120 cm
Gas Plenum Height (metallic fuel only)	90 cm
Average Coolant Density (Pb-Bi)	10.25 g/cm^3

The burnup time steps taken in MOCUP for all cases were one-year steps with no outages. The results for the non-fertile, plutonium-uranium-zirconium (Pu-U-Zr), and plutonium-thorium-zirconium (Pu-Th-Zr) fuels at 300 and 1800 MWe are shown in **Figures 8 and 9**. Note that the Pu-U-Zr fuel has the highest reactivity at BOL and a smaller reactivity swing than the non-fertile fuel. This fuel has the potential for the longest life for relatively similar amounts of added burnable actinides compared to the other fuel compositions. However, the Pu-U-Zr fuel will increase the inventory of plutonium and other actinides in the fuel rather than decrease (or burn) them and the excess reactivity is high at BOL. Therefore, the actinide burning rate and the excess reactivity become major disadvantages for this fuel composition. These disadvantages far outweigh any advantages gained in reactor life. **Figure 10** shows the results for a comparison between metallic fuel (Pu-U-Zr) and nitride fuel (Pu-U-N). The excess reactivity and reactivity swing in the nitride fuel core appear to be smaller than in the metallic fuel (Pu-U-Zr) core, but the same problems exist. The nitride fuel (Pu-U-N) will still breed rather than burn actinides, and still has a higher BOL excess reactivity than the non-fertile fuel.

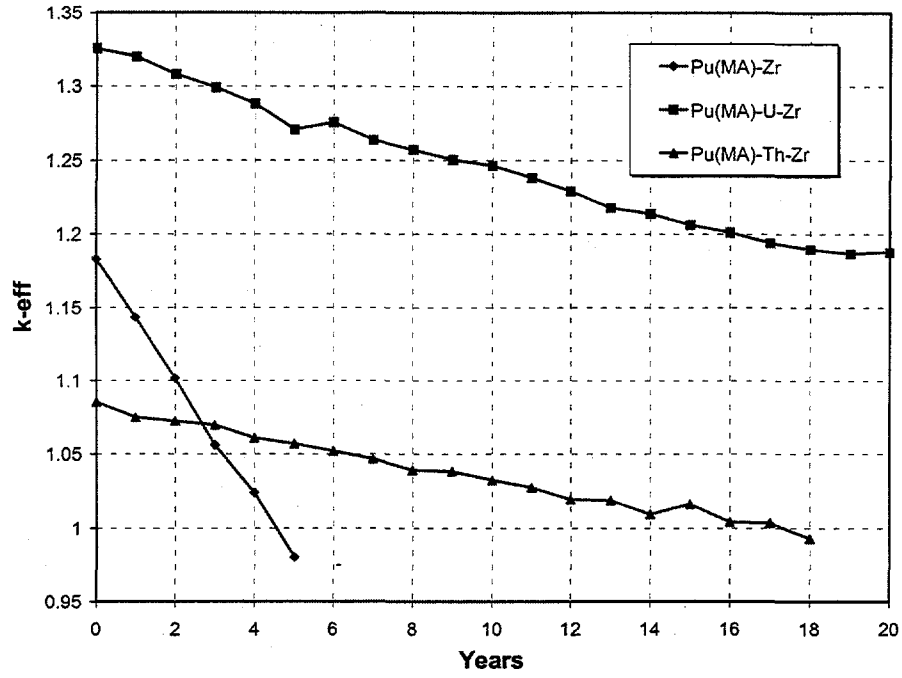

Figure 8. Comparison of metallic fuel types at 300 MWe.

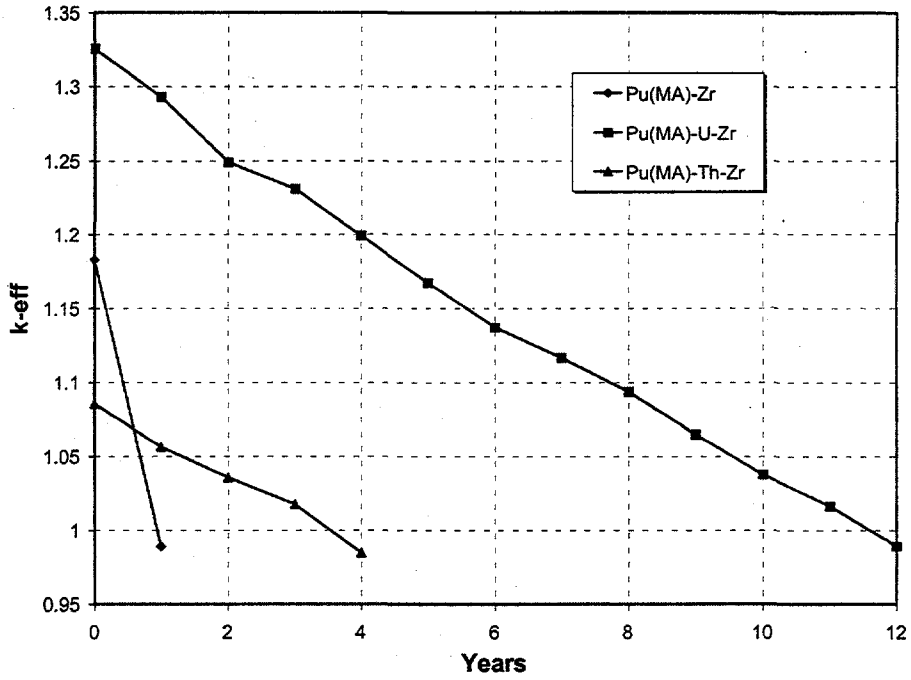

Figure 9. Comparison of metallic fuel types at 1800 MWe.

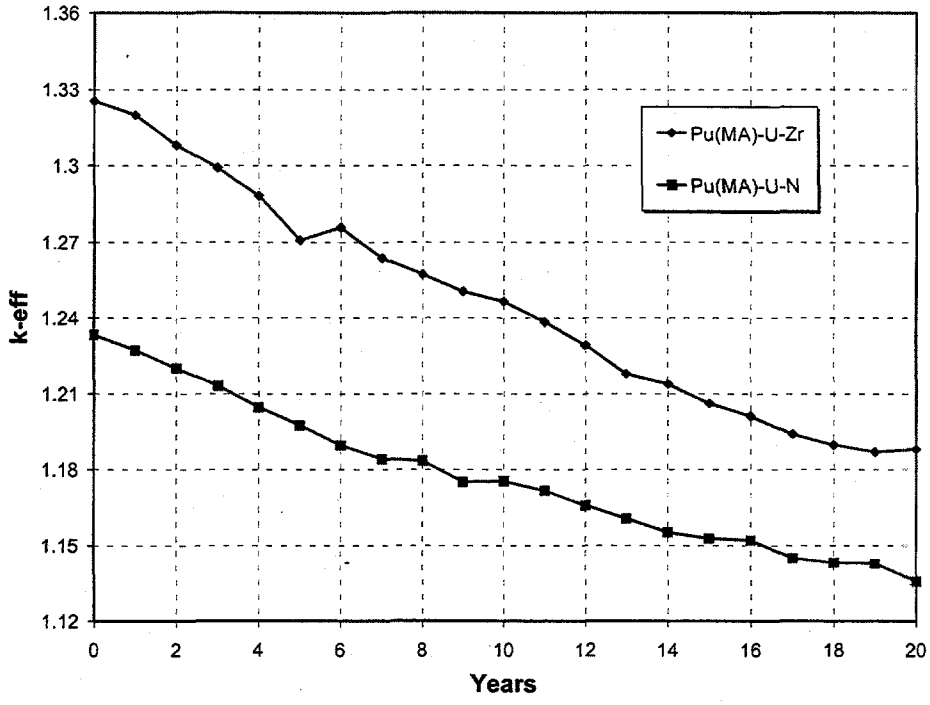

Figure 10. Comparison of metallic and nitride fuel at 300 MWe.

From the results thus far, the optimum mix appears to be the Pu-Th-Zr fuel, although calculations need to be performed on the Pu-Th-N fuel to verify the hypothesis. The Pu-Th-Zr fuel shows promise in that the reactivity swing is slightly smaller than the Pu-U-Zr fuel; the excess reactivity is lower than all other fuel types, therefore, more actinides can be burned in a given cycle; the actinide production (especially plutonium) is much lower; and a relatively long fuel life can be attainted. In other words, because the excess reactivity is low and the reactivity swing remains fairly constant throughout the life of the Pu-Th-Zr fuel, it is possible to add more actinides to increase the cycle length and thereby the burn rate. Note that because U-233 will be present in the Pu-Th-Zr fuel at the EOL, some uranium will need to be added to denature the fuel. Although some plutonium will be produced because of the addition of the uranium, the amount should be minimal.

3.3 Fuel and Materials Selection and Limits (MIT and INEEL)

The reference non-fertile fuel is made of zirconium, plutonium and minor actinides (the weight fraction is 74, 20.8 and 5.2%, respectively). Two different types of fuel form can be considered:

a) A metallic alloy of a zirconium, plutonium and minor actinides. Metallic alloys of zirconium, uranium and plutonium have been the subject of extended studies at Argonne National Laboratory (ANL) in the past two decades. However, in the ANL fuel the main component (i.e. the continuum phase) is always a heavy metal (i.e. uranium and/or plutonium). The presence of a significant amount of minor

actinides and the prevalence of zirconium over Pu, make the selected fuel relatively novel.

b) A dispersion type fuel with coated particles containing about 80 to 90 % TRU and the remainder zirconium in a pure zirconium matrix. The particle coating is yet to be determined, but could be zirconium carbide. Coated particle dispersion fuels are known to have better geometric stability under neutron irradiation and to retain more fission products, especially the gaseous fission products. Therefore, it is likely that a fuel design can be developed that does not require large fuel-to-cladding gaps and metal bonding in the gap. Some work has been done on this type of fuel for space reactor applications.

In the following sections only fuel a) is considered. Since the availability of experimental data for the thermo-physical characteristics of this fuel is scarce, a simplifying assumption is to be made: the properties of the minor actinides are set equal to those of plutonium.

3.3.1 Non-fertile Fuel Melting Temperature

Figure 11 illustrates the phase diagram of the binary alloy Zr-Pu, which provides the melting point and the crystalline configuration of the alloy fuel as a function of the zirconium weight fraction. It can be seen that at reference composition (74% Zr - 26% Pu) the fuel melting point is approximately 1600°C.

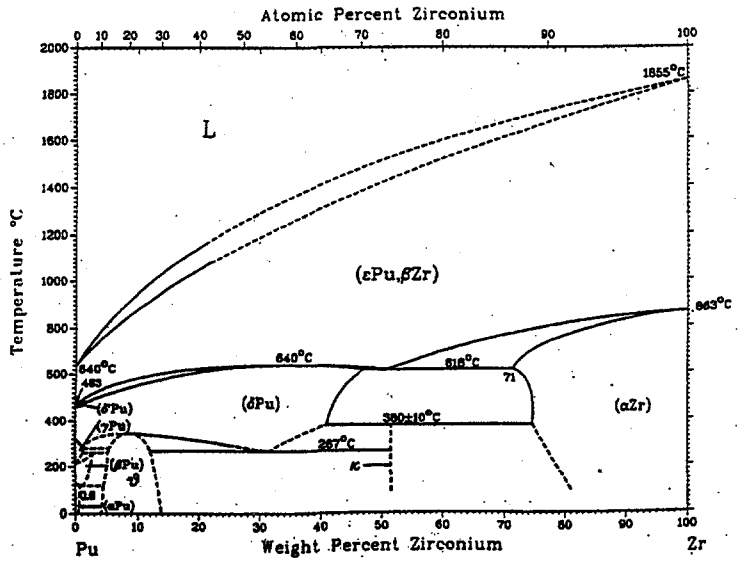

Figure 11. Phase diagram for the zirconium-plutonium binary alloy

3.3.2 Non-fertile Fuel Thermal Conductivity

To evaluate the thermal performance of the non-fertile metal fuel under steady state or transient conditions, it is essential to know its thermal conductivity as a function of temperature and burnup. An estimate of an alloy property can be in principle obtained by taking an appropriate average over its components. Here the thermal conductivity of pure βZr and εPu (see **Figure 11**) are averaged by means of the respective weight fraction to yield the thermal conductivity of the unirradiated fuel at any temperature above 973 K (i.e. 700°C):

$$k = 0.74k_{Zr} + 0.26k_{Pu} = a + b_1 T + b_2 T^2 + b_3 T^3$$

where T is in K and k is in W/cm K.

The value of the numerical coefficients is:

$a = 0.19856$
$b_1 = -1.04439 \times 10^{-4}$
$b_2 = 1.96148 \times 10^{-7}$
$b_3 = -5.00737 \times 10^{-11}$

A benchmark of this method against the experimental values of thermal conductivity of other Pu metallic binary alloys indicates a systematic tendency of this approach to over predict the thermal conductivity with an error of at most 30%.

When the fuel is irradiated, the fission gases fill the pre-existing fuel pores and create new ones. As a result the thermal conductivity decreases. When the number and size of gas filled pores become very large, most pores agglomerate into larger interconnected cavities, which are rapidly filled by the gap bond, leading to a sharp increase of the fuel heat transfer capability.

The pore effect on thermal conductivity (i.e. the burnup effect) can be estimated by means of the following equations [Bauer, 1993]. For gas filled pores only:

$$\frac{k_e}{k} = (1 - P_g)^{(3\varepsilon/2)}$$

where k_e is the thermal conductivity of the irradiated fuel and k is the thermal conductivity of the unirradiated fuel, P_g is the fuel porosity due to gas filled pores and ε is the pore shape factor (ε=1.0 if spherical pores are assumed). The maximum value of P_g (corresponding to the minimum thermal conductivity) was experimentally determined to be 0.25 for the ANL fuel [Bauer et al., 1993]. **Table 5** reports k_e versus the fuel temperature for five different values of P_g.

Table 5. Fuel Thermal Conductivity (W/cm K)

		ε = 1.0 (Spherical Shape)			
T (K)	P_g=0.0	0.05	0.1	0.18	0.25
600	0.195	0.181	0.167	0.145	0.127
700	0.204	0.189	0.183	0.152	0.132
800	0.215	0.199	0.183	0.168	0.139
900	0.226	0.210	0.179	0.178	0.147
1000	0.240	0.222	0.189	0.189	0.156
1100	0.254	0.235	0.201	0.159	0.165
1200	0.269	0.249	0.213	0.200	0.175
1300	0.284	0.263	0.224	0.211	0.184
1400	0.299	0.277	0.237	0.222	0.194
1500	0.314	0.291	0.268	0.233	0.204
1600	0.328	0.304	0.280	0.244	0.213
1700	0.341	0.316	0.270	0.254	0.222
1800	0.354	0.327	0.280	0.263	0.230

3.3.3 Evaluation of Structural and Cladding Materials

The objective of this evaluation is to identify the fuel cladding and structural materials that are compatible with a liquid lead-bismuth cooled, actinide burning fast reactor operated at temperatures from 450 to 650°C, with a cold leg temperature of 450°C, hot leg temperatures up to 600°C, and cladding temperatures of up to 650°C. The liquid lead-bismuth has a eutectic composition (44.5 wt% Pb) which results in a minimum melting temperature of about 125°C.

Iron is present in most structural materials. The solubility of iron in liquid lead-bismuth eutectic varies by a factor of about 20 within the temperature range of interest (450 to 650°C), 1 ppm at 450°C, and 19 ppm at 650°C (Weeks and Romano 1969). The large variation in the solubility introduces a solid-liquid metal interaction in which the principal process occurring is a continuous dissolution of the structural material in the hot regions of the test or reactor loop and precipitation of solid metal in the cold regions. This dissolution/precipitation process is also called liquid metal corrosion.

Past laboratory experiments with a liquid bismuth system (and, therefore, presumably in a liquid Pb-Bi system) have shown that the concentration of the dissolved solid metal in the solution reaches a steady state value throughout the system and is approximately equal to the *solubility of the solid metal (iron) at the lowest temperature* of the solid-liquid interface in the system. This is so because the rate of dissolution of iron into the liquid metal is slower than its precipitation rate. Therefore, the maximum corrosion rate corresponds to the solubility of the solid metal at the maximum interface temperature in the system. The maximum solution rate, R_{max}, can be approximated by

$R_{max} = \alpha_{Tmax} (S_{oTmax} - S_{oTmin})$

Where:

α_{Tmax} = solution rate constant at the maximum temperature
S_{oTmax} = solubility at the maximum temperature at the metal-coolant interface
S_{oTmin} = solubility at the minimum temperature at the metal-coolant interface

The above equation can be used to predict the maximum corrosion rate during a test if the value of α_{Tmax} can be determined from the available test results. For example, from the tests carried out at the Brookhaven National Laboratory with T_{max} = 650°C and T_{min} = 500°C, α_{Tmax} was equal to about 2.13 (Weeks and Romano 1969).

The main concerns in selecting the structural materials for a liquid lead-bismuth fast reactor are their resistance to liquid metal corrosion and their radiation stability. The corrosion tests performed during the last 50 years indicate that liquid metal corrosion can be minimized or eliminated by having a corrosion-resistant, self-healing, surface film (consisting of oxides, carbides, or nitrides) on the structural materials at the beginning of a test, and maintaining it during the test.

In addition to liquid metal corrosion, the structural and fuel cladding materials may be subject to liquid metal embrittlement, erosion-corrosion, low-cycle fatigue, and, depending upon the selected material, radiation-induced creep and swelling, and irradiation-assisted stress corrosion cracking. The following discussion presents a review of the technical literature related to liquid metal corrosion. Available information on the Russian experience in using materials resistant to liquid metal corrosion is also discussed.

Corrosion Tests. Corrosion Tests A progression of static and dynamic tests can be performed to evaluate liquid metal corrosion of structural and fuel cladding materials. The dynamic tests have included spinner tests, thermal convection loop tests, and forced convection loop tests (Branover et al. 1994, Asher et al. 1977, Vreeland et al. 1953). Static tests are generally performed under isothermal conditions and are easy to interpret. In addition, these tests are less expensive than dynamic tests, making them ideal for screening a large number of potential candidate materials. Generally, the materials that are corroded in the static tests are likely to corrode more in the dynamic tests.

There are four factors that may affect liquid-metal corrosion in static tests: temperature, the ratio of the specimen surface area to volume of the liquid, the purity of the liquid metal, and the surface condition of the candidate material, such as the presence of grain boundary precipitate (Manly 1958). It is essential that the isothermal condition of the test should be closely controlled.

Static test results may be evaluated using following methods:

- Visual and low-power microscopic examinations of specimen and corrodant.
- Weight change data on specimen.

- Metallographic examination of specimen and sections of specimen for type and extent of corrosion attack
- X-ray and spectrographic identification of surface layers that were formed before test or during test.
- Chemical analysis of the corrodant after the test for content of the specimen metal.

Spinner tests have been performed to evaluate the effects of high relative velocity on corrosion and erosion of various candidate materials. These tests may employ relatively high velocities (450 m/min) achieved by rotating specimens in a pot containing the liquid metal at isothermal conditions (Branover et al. 1994). Thermal convection loops have also been useful in mass-transfer studies. Flow of the molten metal is achieved by heating one leg of the loop, for example, to 600°C and other leg to lower temperature (450°C). Flow velocities of 6-10 ft/min are possible.

Asher et al.(1977) used a simple laboratory scale loop, based on the design of Cathcart and Manly (1954), for containing liquid lead. The loop was made from silica glass, which has proved to be very resistant to attack by molten lead, provided ingress of oxygen is prevented. Such a silica loop may be used if it is also found to be resistant to liquid lead-bismuth. Asher et al. had made some modifications to the loop design so that it can be used for static tests, spinner tests, and thermal-convection tests.

The most realistic type of dynamic test is the forced circulation loop that can be made to reproduce actual operating conditions. The heat is supplied by electric heaters and removed by means of air jets, if necessary, to obtain large temperature gradients. Pumping of liquid metal can be done by means of an electromagnetic pump. The flow velocity in operating reactors can be as high as about 2.5 to 3 m/s. The forced circulation loop should be designed to avoid cavitation at high velocities, where the velocity head may exceed the pressure head.

The factors that affect the liquid metal corrosion rate in dynamic tests, in addition to the ones mentioned for the static tests, include flow velocity and the temperature difference seen by the coolant (Manly 1954).

In addition to the evaluation methods for the static test results, the evaluation methods for the dynamic test results may include following:

- Examination and identification of the crystals that often form plugs in these tests.
- Evaluation of the effects of different velocities on the rate of erosion-corrosion.
- Evaluation of the effects of loop geometry and high flow velocities on cavitation-erosion.
- Study of the effects of high residual and applied stresses on the possibility of liquid metal embrittlement. Asher et al. (1977) accomplished this by applying high tensile stress to rotating specimen in their spinner tests.
- Studies of the effects of cyclic stresses on fatigue resistance

In summary, a complete evaluation of the structural and fuel cladding material for a liquid lead-bismuth cooled reactor might consist of first a static corrosion test; second,

spinner tests; third, thermal convection tests; and finally, forced circulation loop tests. This order of testing is the one in which the severity of the test, the difficulties in the experimental techniques, and cost of operation gradually increase. If a material fails in one of the tests, it has been found by experience that it is likely to fail in the more severe tests that follow.

Corrosion Protection with Surface Films. Corrosion Protection with Surface FilmsTo minimize liquid metal corrosion of structural steel, it is essential that the protective film is stable and easily repairable in the liquid lead-bismuth cooled reactor environment. Our review of the literature has identified the following five requirements for a film at the interface between a specimen and a lead-bismuth melt:

1. The film constituents have large, negative, Gibbs free energies in the operating temperature range.
2. The thermal expansion coefficient of the film matches well with that of the substrate.
3. The film thickness is small.
4. The film is readily reparable.
5. The film has adequate resistance to radiation and fission products.

The first criterion ensures that the film, once it is formed, is stable, whereas the fourth criterion ensures that the kinetics of film formation are fast enough so that the films can be readily repaired. The fourth criterion also implies that a sufficient supply of the constituents of the film (such as O_2, N_2, C, Fe, Si, Zr, Cr) are readily available at the interface. The second and third criteria ensure that the film will not crack easily during operation. The out-of pile corrosion tests discussed earlier can be used to evaluate the first four criteria. In-pile tests will be required to evaluate the fifth criteria.

A film satisfying the above criteria may consist of oxides, nitrides, or carbides of certain elements (such as Fe, Cr, Si) present in the structural materials (ferrous alloys and stainless steels), or of certain other elements (such as Zr, Ti) added externally. As discussed next, the film may be formed prior to the test by an oxidizing, carburizing, or nitriding process, or during the test provided a proper partial pressure of oxygen is present or appropriate inhibitors are added to liquid lead-bismuth pool.

Oxide Films. Iron, chromium, silicon, aluminum, and several other oxides have higher negative free energy of formation than those of the lead and bismuth oxides, as shown in **Table 6.** Therefore, lead and bismuth oxides can not reduce these oxides over the range of temperatures of interest. If an oxide film is present on a steel specimen, oxygen diffusing toward the specimen may strengthen this film; this process is strongly influenced by the temperature and the partial pressure of the oxygen. (If an oxide film is not present, then the oxygen from the liquid metal diffuses into the steel and causes internal oxidation. In addition, the steel may be damaged by liquid metal embrittlement.)

Table 6. Free Energies of Formation of Nitrides, Carbides, and Oxides at 600°C (-ΔG, Kcal/mol of N, C, O)[a] (DeHoff 1993)

Nitride	-ΔG	Carbide	-ΔG	Oxide	-ΔG
ZrN	66.91	Cr_7C_3	51.26	Al_2O_3	313.07
AlN	54.24	ZrC	45.78	ZrO_2	222.11
UN	46.23	TiC	41.28	Cr_2O_3	215.09
CrN	11.06	SiC	14.76	Fe_3O_4	195.94
Fe_4N	-7.83	WC	8.74	SiO_2	178.92
		Fe_3C	-1.76	$FeCr_2O_4$	?

[a] Free energy estimates do not include contributions from changes in heat capacities with temperatures. Some of the free energy estimates vary significantly from those provided by Taylor (1956).

The composition of the oxide film formed on a given steel depends on temperature and the oxygen partial pressure. For example, consider the oxidation of chromium-nickel steel similar to Type 304 stainless steel. At 600°C, both Fe_3O_4 and $FeCr_2O_4$ can form. But at a very low oxidizing potential (very low oxygen content), only $FeCr_2O_4$ (spinel) forms. The spinel provides a much better resistance to liquid metal corrosion and embrittlement as compared to Fe_3O_4 (Bichuya 1969). However, this low oxygen content might not be sufficient for ready repair of the damaged film as discussed next.

The oxide film can provide adequate protection against liquid metal corrosion provided it is readily reparable. Both an adequate oxygen supply and metal ions should be readily available to repair the damaged oxide film. To illustrate the point, we will describe the corrosion test results for Croloy 2 (Asher et al. 1977). A Croloy 2 specimen was oxidized in air at 450°C for 1 hour. The resulting oxide film thickness was about 3000 A. Then part of the surface was abraded to remove a portion of the oxide film. Then it was tested in liquid lead at 700°C for 29 days. Subsequent examination showed that the specimen was heavily pitted. The likely reason for this corrosion was that the lead had a very low oxidizing potential during the experiment since it was continuously being reduced by a hydrogen/argon blanket gas. Thus any flaw in the otherwise protective film would not be self-healing. This situation contrasts with that often found industrially where the molten lead is not completely protected from contact with air or other sources of oxygen. Hence, the lead has a high oxidizing potential and is able to cause healing of flaws in the oxide films on ferrous alloys used to contain it.

The addition of silicon to ferrous alloys may be beneficial because silica (silicon oxide) has a large, negative, free energy. However, sufficient amount of silicon should be present in the steel so that the damaged oxide film can be readily repaired. Asher et al. (1977) tested this idea on Tanitron, a cast iron containing 13.5 wt% Si. The specimen showed no sign of attack and no significant change in weight or in length after exposure to liquid lead at 720°C temperature for 56 days. The following test results suggest that we may not need silicon as high as 13.5 wt%, 1 wt% may be sufficient. Tsirlin et al. (1998) tested Type 316 L stainless steel (1 wt% Si, 10-14 wt% Ni) samples at 500°C in liquid lead covered with nitrogen at a certain partial pressure of oxygen. The oxygen partial pressure was sufficient to form PbO and make the liquid lead saturated with oxygen. This high oxygen content will facilitate rapid formation of an oxide film. Examination of samples at different stages of testing revealed that the concentration of Fe, Ni and Cr near the sample surface did not change during the test period (up to 800 h). At the same time, complex oxide phases (spinels and silicates) were found on the sample surfaces. The formation of these oxides was the reason for the high stability of Type 316 L SS samples in liquid lead and the absence of selective solution of nickel in lead. (Ni has a high solubility in liquid lead compared to Fe and Cr, but the composition of the steel substrate remained unchanged.) The effect of selective solution (leaching) of Ni is observed at a very low activity of oxygen in liquid lead, possibly because of slow kinetics of oxide formation and/or repair.

It appears that 1 wt% Si in a stainless steel composition may be sufficient for the formation and repair of silicate films. The silicone content in the Russian Fe-Cr steel (EP 823), successfully used as structural and cladding material for their liquid Pb-Bi submarine reactors (apparently operated at temperatures below 480°C), is in the range of 1 to 1.3 wt%. The chemical composition of EP 823 is given in **Table 7**. The Russian experience indicates that 10^{-7} to 10^{-9} wt% of oxygen in the liquid lead-bismuth coolant is sufficient to protect this material from liquid metal corrosion. It appears that the oxygen content is kept high so that the oxide film can be formed rapidly at the beginning of use and repaired readily as needed. However, it appears that the high oxygen content leads to formation of lead and bismuth oxides over time, and the reactor coolant has to be exposed to a strongly reducing environment (hydrogen injection) every one to three years to breakdown the lead and bismuth oxides (Chitaykin 1999). Also, proper distribution of the hydrogen requires a coolant flow rate of at least 1 meter/sec, and no flow stagnation at any location within the system. Therefore, the primary system must be a forced (pumped) flow system. Forced flow is also required to provide a uniform oxygen content everywhere in the primary system. Special filters are also needed for removing admixtures that cannot be reduced chemically.

Table 7. Chemical Composition of Potential Candidates for Structural and Fuel Cladding Materials

Material	C	Si	Mn	S	P	W	Cr	Ni	Mo	V	Nb
EP 823	0.14 0.18	1.0 1.3	0.5 0.6	NC	NC	0.5 0.8	10.0 12.0	0.5 0.8	0.6 0.9	0.2 0.4	0.2 0.4
HT-9	0.2	0.2	0.6	0.03	0.04	0.5	12.0	0.5	1.0	0.3	....
436 SS	0.12	1.0	1.0	0.03	0.04	....	16.0 18.0	....	0.75 1.25	...	**

NC - not clear; ** 5 x %C min Nb + Ta

Other candidates for the structural and fuel cladding material are HT-9 steel and ferritic stainless steels such as Type 436 stainless steel. The chemical compositions of these steels are also presented in **Table 7**. There is some reservation about HT-9 steel because its low silicon content (0.2 wt%) may not be adequate to form and maintain a silicate film on a specimen surface exposed to Pb-Bi melt at operating temperatures (450 to 650°C). However, spinel ($FeCr_2O_4$) can be formed and may be sufficient to provide corrosion protection. The HT-9 steel has low Ni, so radiation-induced swelling will not be a concern.

The chemical composition of Type 436 stainless steel is somewhat similar to that of EP 823. However, the absence of Ni raises some concern about its fracture toughness. This needs to be further investigated.

Nitride and Carbide Films. Several nitrides and carbides, especially zirconium nitride (ZrN) and carbide (ZrC), have a higher negative free energy of formation than those of chromium and iron nitrides, as shown in **Table 6**. Advantage of this fact is taken by adding zirconium as an inhibitor in the liquid metal at ppm levels. The added zirconium reacts with the small amount of nitrogen and carbon present in the steel and forms a protective, inert layer of ZrN and ZrC. Which of these films will form on the surface is determined by the relative activities of the C and N in the steel, and these in turn are functions of the steel composition and heat treatment. Thermodynamically, ZrN is appreciably more stable than ZrC; the free energies of formation at 550°C are estimated to be -67 Kcal/mole for ZrN and -46 Kcal/mole for ZrC, as calculated from the data given in DeHoff (1993). Electron diffraction examination of the surface films on uncorroded steel specimens from a large liquid-bismuth loop showed that the principal protective compound is ZrN (Horsley and Maskrey 1958).

Thermal convection loop tests have shown that inhibition cannot be maintained if the Zr concentration is less than 100 ppm. Several liquid-bismuth loop experiments at Harwell have indicated that about 200 ppm Zr was insufficient to repair (reform) the protective film. The maximum Zr concentration that can be used is determined by the solubility of Zr at the lowest temperature of operation.

The solubility of Zr in the liquid lead-bismuth eutectic under isothermal condition and at equilibrium is given by following equation:

$$\log_{10} (\text{ppm Zr}) = 6.15 - (3172/T)$$

over the temperature range of 350-750°C (Weeks and Romano 1969). The temperature, T, is in degree Kelvin. The solubility of Zr at 400 and 650°C is 27 and 516 ppm, respectively. This equation may not be applicable to a forced-flow liquid lead-bismuth cooled reactor system during operation because dynamic conditions rather than static equilibrium and isothermal conditions are present during plant operation. So the effect of plant operation on the solubility of the zirconium needs to be evaluated.

If oxygen is present near the ZrN film, it will react with the film and convert it to tetragonal zirconia, which readily breaks away from the steel surface. Oxygen can come from the melt or through a weld in a steel loop if the weld contains fine pores and cracks along which oxygen can travel to the liquid metal-steel interface. Magnesium may be added to liquid metal to act as a getter (scavenger) for oxygen.

A zirconium nitride film may provide only temporary protection to steel, it is liable to spall off and not reform. This results in localized corrosion attack on the underlying steel. This problem can be addressed by increasing the nitrogen content in the steel from typically 0.1 wt% to 1.0 wt%. This increase in the nitrogen content enhances the corrosion resistance of the film in two ways: (1) it reduces imperfections in the nitride film. The imperfections are due to reactions between Zr and phosphorus, sulfur, carbon, and other nonmetallic inclusions present in the steel. The reaction products reduce the ability of the ZrN film to adhere to the steel surface. (2) It provides a supply of nitrogen for film repair (Horsley and Maskrey 1958). However, nitrogen in the steel takes some time to diffuse to the interface, so it may not be readily available. As an alternate solution, the steel specimens may be nitrided prior to the test. A thin film of Zr is placed on the specimen surface, then the specimen is placed in dry ammonia atmosphere at elevated temperature. This nitriding process ensures that an ample amount of nitrogen is present at the interface and available for ready repair.

The thermal expansion coefficient of ZrN is approximately that of steel between 17 and 680°C; therefore, as the ZrN films become thicker their sensitivity to spalling upon temperature change is expected to increase. Therefore, a ZrN film should be as thin as possible so that it does not break easily, but it should be thick enough to provide adequate corrosion protection.

3.4 Core Thermal-Hydraulics (MIT)

3.4.1 Core Geometry

The thermal analysis of the fuel is based on the core geometry illustrated in **Figures 1** and **2**. Numerical values of the parameters are reported in **Table 8**. The selection of the core geometric characteristics and the fuel composition are mainly driven by neutronics requirements (see Section **3.1**).

Table 8. Core geometry including fuel dimensions, number of fuel assemblies, and composition.

Fuel pellet OD	8.64 mm
Fuel composition (wt%)	26% of Pu+actinides, 74% of Zr
Gap thickness (at BOL)	0.2 mm
Bond material - lead-bismuth-tin alloy (wt%)	33%Pb-33%Sn-33%Bi
Cladding thickness	0.63 mm
Cladding material	Stainless steel EP-823
Pin outer diameter	10.3 mm
Pitch	12.55 mm
pitch to diameter	1.2
Heated core length	1.3 m
Gas plenum height	1 m
Number of fuel assemblies	157
Number of fuel assemblies with control	53
Number of fuel rods per assembly	240
Core barrel inner diameter	4 m

3.4.2 Temperature Limits

The presence of a significant amount of minor actinides makes the selected fuel relatively novel. As discussed in Section 3.3, a simplifying assumption is made: to a first approximation the thermo-physical and thermodynamic properties of the minor actinides can be set equal to those of plutonium. This assumption enables the use of the ANL data on the characteristics of Pu-Zr binary alloys.

Figure 11 illustrates the phase diagram of the Pu-Zr alloy. It can be seen that the alloy melting point (along with its crystalline stability) significantly increases with the Zr weight fraction: at 74wt% Zr, the melting point is approximately 1600°C. Somewhat below this value is then the fuel temperature design limit. Since the fuel-clad gap is designed to allow for partial fuel restructuring, the phase transition at approximately 700°C does not set a serious limit on the fuel temperature.

Review of the existing literature on the stainless steel EP-823 corrosion by Pb-Bi indicates that the maximum allowable temperature is approximately 650°C. This is then the cladding outer surface temperature limit tentatively selected in this project. Corrosion

of EP-823 is inhibited by the formation and maintenance on the steel surface of an oxide layer whose integrity significantly depends on the Pb-Bi temperature, flow rate, and oxygen content as well as the minor alloy constituents in the cladding, especially the silicon and vanadium concentrations. The lack of Western experimental data and theoretical study on the physics of this oxide layer make the above temperature limit subject to uncertainty.

Moreover, because the thermo-physical properties of EP-823 are not readily available, they were set equal to those of HT-9, whose composition resembles it (but with less silicon, see **Table 7**).

3.4.3 Basic Assumptions

The variation of the fuel thermal conductivity with burnup displays a minimum at 25% porosity. The mechanism leading to a minimum is briefly described as follows: the thermal conductivity initially decreases with burnup as the released fission gases increase the fuel porosity. When the number and size of gas filled pores become very large (i.e. above 25%), most pores agglomerate into larger interconnected cavities, which are rapidly filled by the gap bond, leading to a sharp increase of the fuel heat transfer capability. To avoid computational complications, the thermal conductivity of the fuel is conservatively assumed to be constant with burnup and equal to this minimum value. For a theoretical estimate of the fuel thermal conductivity, refer to Section **3.3**. Convective effects in the gap are neglected hence heat is transferred through the thin liquid metal bond by conduction only.

Several correlations developed for liquid metal flow in rod bundles were considered for the calculation of the Pb-Bi heat transfer coefficient on the outer surface of the clad. The Westinghouse correlation [Kazimi and Carelli, 1976] consistently yields the most conservative values of the heat transfer coefficient and it was then chosen for this analysis.

Depending on the primary system configuration and on the reactor thermal power, the average coolant velocity in the core ranges from 0.5 to 2.5 m/s (see Section **3.5**). If the total core thermal power is assumed to range from 1500 to 2000 MWth, the average linear heat generation rate in the fuel pins ranges from 31.2 to 41.6 kW/m. The radial and axial power peaking factors are assumed to be 1.17 and 1.6, respectively (see Section **3.1**). Therefore the peak linear heat generation rate ranges between 58.4 and 77.9 kW/m, corresponding to 1500 and 2000 MWth, respectively. If the control rods are inserted from the core bottom[4], the axial power peak takes place at the core exit and the highest fuel and clad temperature are expected here. The coolant bulk temperature at the core exit is assumed to be 550°C because it will be demonstrated (see Section **3.4**) that core outlet temperatures about this value are necessary to obtain effective natural circulation in the primary system.

[4] This might be the preferred location due to the buoyancy of control materials in the heavier Pb-Bi coolant.

3.4.4 Results and Discussion

In **Figure 12** the fuel centerline temperature and the clad outer temperature of the hot channel are plotted as a function of the local linear heat generation rate for three different values of the coolant velocity.

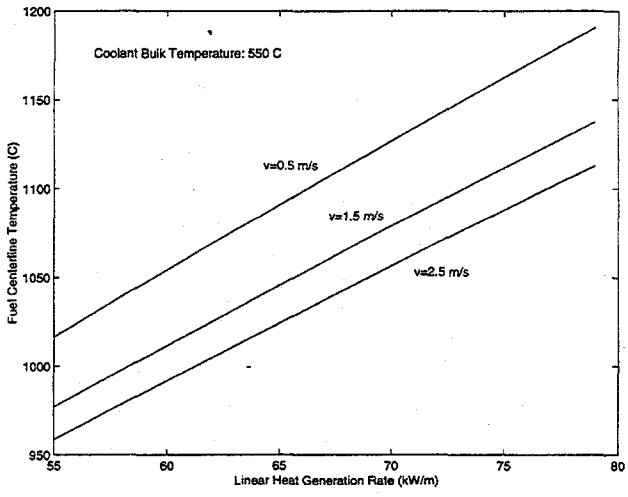

Figure 12a

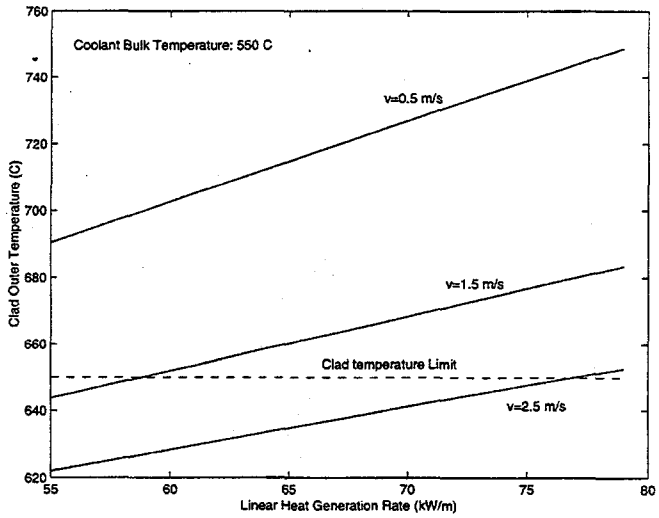

Figure 12b

Figure 12. Fuel centerline temperature (Figure 12a) and cladding surface temperature (Figure 12b) as a function of linear heat generation rate at three coolant velocities.

The maximum temperature within the fuel is considerably below the fuel melting point (i.e. 1600°C) under all circumstances. As expected, the cladding sets the most severe limit: the temperature on the outer surface of the clad appears to be unacceptably high for Pb-Bi velocities smaller than 2.5 m/s. This value of the coolant core velocity can be attained only if:

a) the primary coolant is actively pumped through the core, or

b) a gas-pump scheme is adopted (see Section **3.5.6**), which enables achievement of very effective passive circulation in the primary system.

In any case a factor of 1.6 axial power peaking (especially if occurring at the core outlet) is too large and means to reduce it should be explored.

3.4.5 Control Rod Cooling

The control rods are heavily irradiated by fast neutrons and gamma radiation, which will generate considerable heat. Additional heat is deposited as a consequence of the neutron absorption reactions. The magnitude of heating mainly depends on the material scattering and absorption cross sections (for the neutron interactions) and on its atomic number and density (for the gamma interactions). If adequate cooling is not provided, the control system may be unable to appropriately perform its function hence degrading the overall safety of the reactor.

Let us distinguish between two different sets of control rods.

1) The control rods for fine reactivity control have the main purpose of compensating for reactivity decrease with burnup in order to maintain criticality. At BOL these rods are well inserted in the fuel and they are subjected to large heat deposition. If they are immersed in the primary coolant, the heat is effectively removed by convection and conduction. However, a concern exists regarding the deposition of corrosion products and other debris (normally present in the primary coolant) on the control rod driving mechanisms that would decrease the system reliability. To mitigate this concern, it may be desirable to place these control rods in empty channels. In this case the dominant heat removal mechanism is radiation, which does not appear to be effective enough to keep the control rod temperature within acceptable limits.

2) The scram control rods are located above the core. To minimize the probability of scram failure, these rods are placed in empty channels that ensure rapid gravity insertion into the core. Under normal operating conditions, they are kept outside the core. As a result, the heat deposition is small.

Several neutron absorbing materials were explored as potential candidates for the control system. Special attention was given to B_4C because of its relatively large absorption cross section at high neutron energy and to hafnium because of its absorption

resonances that may be used to improve the doppler reactivity feedback. Gamma and neutron heating of control rods made of these two materials were computed by means of the MCNP code. The linear rate of heat deposition ranges from 4 kW/m to 10 kW/m depending on the material (i.e. higher gamma heating in Hf, higher neutron heating in B_4C) and on the location of the control rods. It would be extremely difficult for radiation cooling to remove such a high linear power. As a result, the fine reactivity control rods will likely have to be kept immersed in the primary coolant.

3.5 Primary System Concept and Vessel (MIT)

The reactor core and the Pb-Bi/He heat exchanger are integrated in a pool design. The pool configuration minimizes flow resistance, making natural circulation more feasible, and it offers a better thermal inertia that will moderate the temperature rise that occurs upon loss of the heat sink. Additionally, it facilitates maintenance of the coolant temperature above its freezing point (~125 °C) and helps achieve a more compact layout of the plant.

A reference schematic of the reactor pool is illustrated in **Figure 13.** The gravitational head H is a design variable mainly driven by natural circulation considerations. For the geometric characteristics of the heat exchanger, see Section 3.6.2.

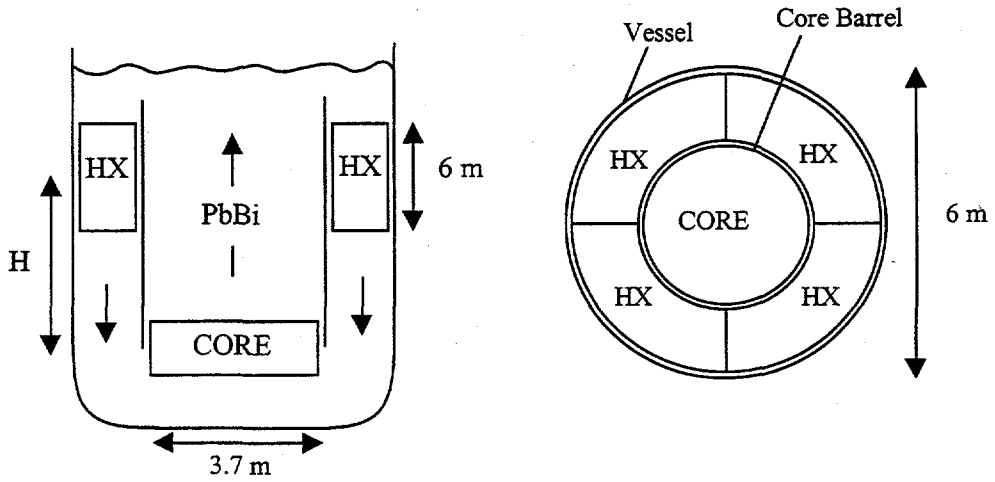

Figure 13. Sketch of the reactor pool and heat exchanger geometry.

3.5.1 Natural Circulation Analysis

The effect of the pitch-to-diameter ratio and gravitational head on the average power density removable by means of natural circulation are explored for the following reference conditions (consistent with the core geometry proposed in Section **3.1**):

- PbBi core inlet/outlet temperature: 250°C/550°C.
- Fuel pins: OD=10.3 mm, Active Length=1.3 m (+1.0 m gas plenum).
- Fuel pins arranged on a square lattice.
- Three spacing grids together with the stiffening provided by the voided streaming tubes shown in Figure 1 to ensure proper separation of the fuel pins.

Figure 14 illustrates the relevant results. The analysis shows that:

a) For relatively large p/d, average power density comparable to sodium cooled fast reactors (up to 50% of French Superphenix) can be achieved, which proves the excellent natural circulation potential of the lead-bismuth eutectic.
b) A core with diameter limited to 4 m can be designed (at 1,800 MWth).
c) Average coolant velocity in the core ranges from 0.5 to 1.0 m/s. In this velocity range the heat transfer coefficient varies between 10 and 12 kW/m^{2}K.
d) Average linear power up to 40 kW/m is obtained.

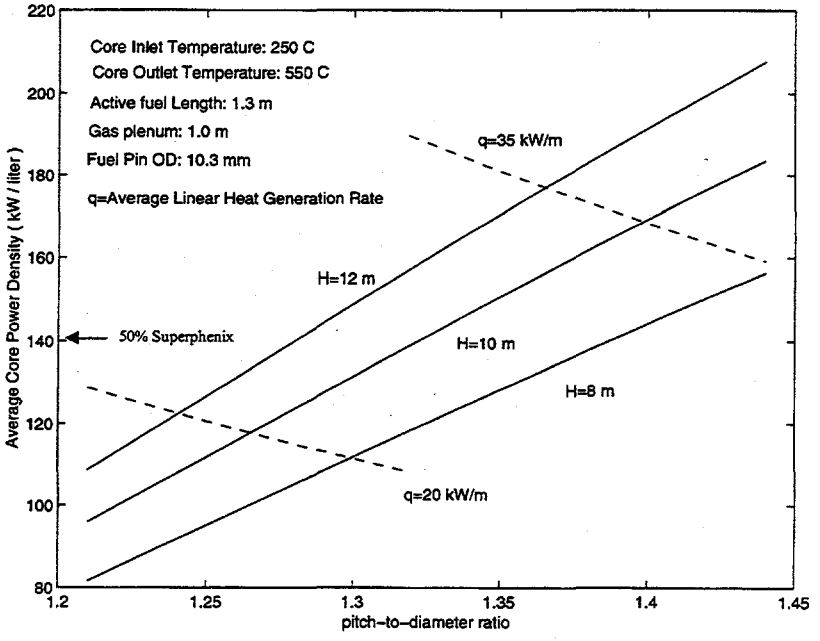

Figure 14. Average core power density as a function of pitch-to-diameter ratio and gravitational head for an active fuel length of 1.3 m.

On the other hand:

a) The neutronic stability of the core seems to favor a very tight lattice (p/d around 1.2), which would deteriorate the natural circulation capability of the system.

b) Given the large axial power peaking, an average linear power above 40 kW/m implies peak linear powers above 60 kW/m. It was shown in Section 3.4.4 that a high Pb-Bi velocity (well above 1.0 m/s) is needed to remove this magnitude of thermal load.

3.5.2 The Effect of Fuel Length on Natural Circulation

To achieve a large negative void reactivity coefficient, the fuel length can be reduced to increase the axial neutron leakage upon voiding. Alternatively, the core diameter can be greatly reduced to increase radial neutron leakage upon voiding. In this case, if the total thermal power is to be kept constant, the fuel active length must be increased leading to a core shape that significantly differs from the reference one (i.e. cigar shape core vs. pancake shape core). **Figure 15** illustrates the power density that can be removed by natural circulation if the fuel length is increased to 3 m. **Figure 16** illustrates the simple geometrical relation between the power density and the core diameter for a 1,800 MWthh total power.

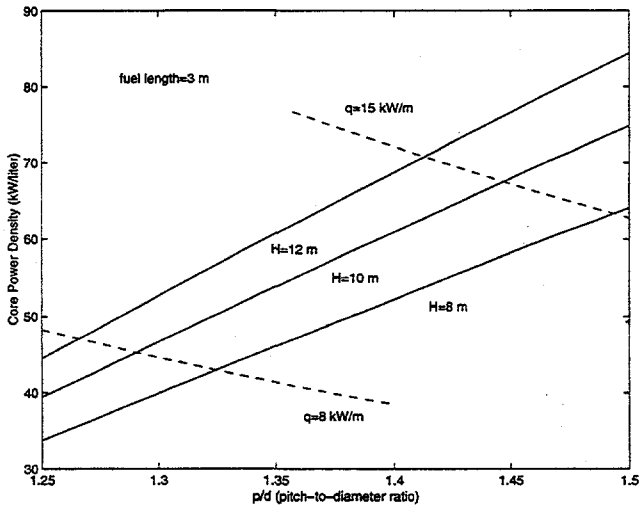

Figure 15. Average core power density as a function of pitch-to-diameter ratio and gravitational head for an active fuel length of 3 m.

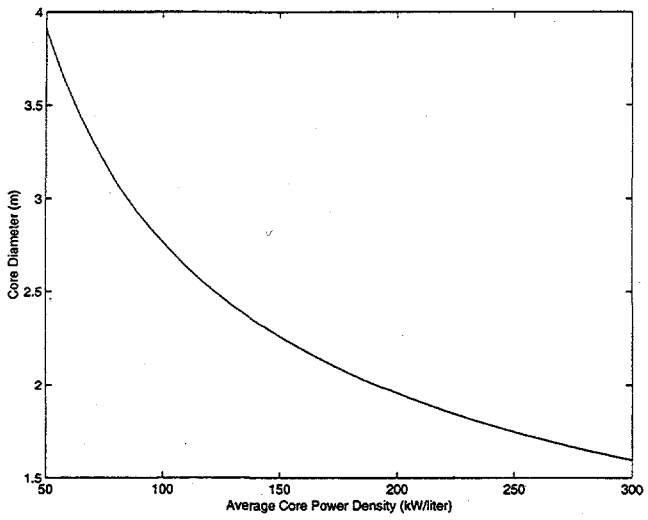

Figure 16. Relationship between power density and core diameter for a 1,800 MWth core.

The results clearly show that the cigar shape core cannot be designed to operate on natural circulation only. The achievable power density is rather small and requires a large core diameter, which defeats the initial purpose of increasing the radial neutron leakage.

3.5.3 Core Voiding as a Result of Secondary Coolant Entrainment upon Rupture of a Heat Exchanger Tube

In Section 3.1 it was shown that the proposed core configuration achieves a negative reactivity coefficient when the coolant is totally or partially displaced from the core. Although this feature greatly mitigates the consequences of coolant voiding, it is also of interest to assess the likelihood of occurrence of this event. When a tube of the heat exchanger fails, the secondary coolant is discharged at high velocity into the reactor pool. A simple (although very conservative) way to evaluate the maximum vertical penetration of this fluid within the Pb-Bi and therefore to assess whether gas can reach the core inlet, is to set the velocity head of the discharged secondary coolant equal to the static pressure of the primary coolant as illustrated in **Figure 17**.

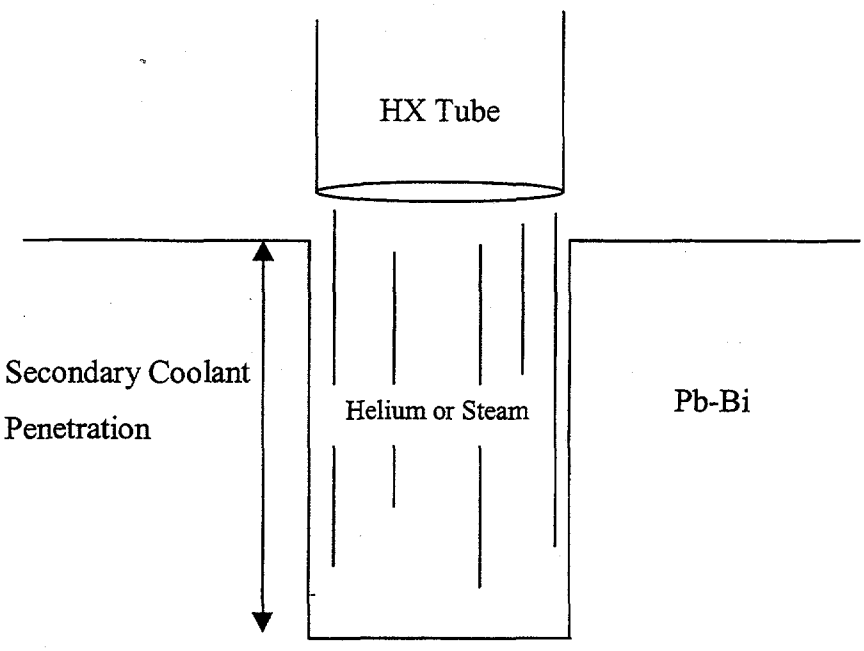

Figure 17. Depth of secondary coolant penetration.

For helium at 7.0 MPa and for steam at 7.0 MPa, the penetration in the Pb-Bi pool is estimated to be 25 and 18 m, respectively, which is greater than the downcomer length of approximately 15 m.

Clearly the possibility of core voiding cannot be ruled out on the basis of this overly simple model that ignores the effects of viscosity and the two dimensional nature of a gas jet injected into a stagnant liquid. It may be possible to rule out this scenario using a more realistic estimate of penetration distance from a more sophisticated fluid dynamic model.

3.5.4 Vessel Structural Analysis

The reactor vessel constitutes one of the main barriers to the release of radioactivity. It is essential to ensure that the design temperature limit of the reactor vessel is not exceeded under normal or accident conditions. The vessel material is assumed to be EP-823 stainless steel, whose mechanical characteristics are inferred from those of HT-9. The structural analysis satisfies the requirements of the ASME code case N-47. **Figure 18** shows the HT-9 allowable design stress intensity vs. temperature curve. The dependence of the design stress intensity on the operating time is a consequence of the importance of thermal creep at high temperature (above 450°C).

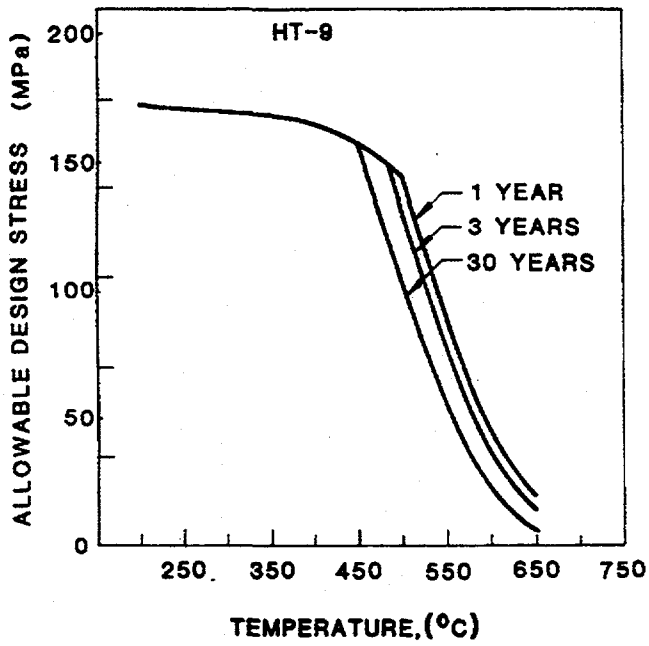

Figure 18. Allowable design stress versus temperature for HT-9 stainless steel.

The vessel is subjected to the following loads:

a) Operating pressure. Due to the high density of PbBi, the operating pressure varies linearly from 0.1 MPa (i.e. atmospheric pressure) at the vessel top to approximately 1.8 MPa at the bottom of the lower head.
b) PbBi and vessel weight.
c) Radial temperature gradient across the vessel thickness (especially when the decay heat is discharged through the vessel, see Section **3.5**). It should be noted that in this structure the radial temperature gradient induces hoop and axial thermal stresses whose average over the vessel thickness is zero. These stresses have to be taken into account in a fatigue analysis only. Since the expected frequency of use of the Decay Heat Removal System is very low, fatigue considerations are relatively unimportant and to a first approximation the thermal load can be neglected.
d) Fast neutron flux. Depending on the downcomer thickness (from 50 to 100 cm), the fast neutron flux (E_n >1MeV) at the vessel surface can range up to 1.8×10^{12} n/cm^{2}s, leading to a total fluence over 30 years of vessel lifetime up to 1.7×10^{21} n/cm^2. The corresponding dose effect is 1.7 dpa.

The vessel beltline thickness is varied between 3 and 10 cm (with a reference value of 5 cm). The thickness of the lower head is selected to be 2/3 of the beltline thickness to minimize the discontinuity stresses. Thin shell theory is applied to find the primary membrane stresses, the discontinuity membrane and bending stresses, the elastic, thermal and irradiation creep strains and displacements. The results of the analysis show that irradiation creep and swelling are negligible. Irradiation embrittlement is expected to shift the Ductile-To-Brittle-Temperature by at most 10°C.

As expected, the mechanical stresses (induced by the operating pressure and the structure weight) decrease as the vessel thickness increases. Since the strength of the material is a decreasing function of temperature (as shown in **Figure 18**), lower stresses enable operation of the vessel at higher temperature: the vessel temperature limit as a function of the vessel thickness is illustrated in **Figure 19**. The design point tentatively selected is 5 cm, corresponding to a maximum allowable temperature of approximately 530°C.

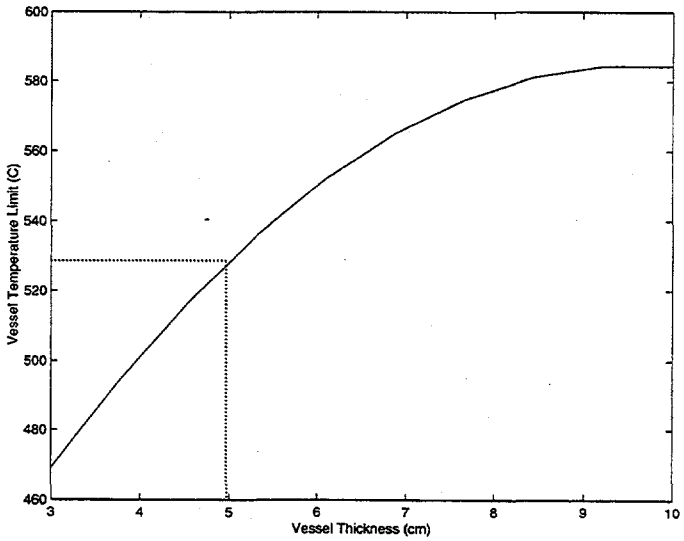

Figure 19. Vessel temperature limit as a function of vessel thickness.

3.5.5 Primary Coolant Capital Cost

Bismuth is a relatively expensive material. Its impact on the cost of the electricity produced by this reactor was evaluated.

Assuming a reactor pool of 15 m height and 6 m diameter, 75% filled with primary coolant, the required Pb-Bi inventory is approximately 3,030 metric tons. Assuming a plant net electric output of 600 MWe, the coolant mass per unit electric power is approximately 5 ton/MWe. The market cost of bismuth is around 7 $/kg and that of lead is around 1 $/kg. The lifetime of the coolant is assumed to be 25 years. The after-tax averaged cost of capital is 8%. Disposal cost or salvage value are not considered.

Table 9 compares the capital cost of lead-bismuth coolant and pure lead coolant for two different values of the capacity factor f.

Table 9 Coolant levelized capital cost (mills/kWh)

	f=0.6	f=0.9
Pb-Bi	0.53	0.35
Pure Pb	0.12	0.08

As can be seen, the cost of PbBi is not negligible. Nevertheless, it is approximately a factor of 5 less than the cost of the D_2O inventory for a CANDU reactor.

3.5.6 An Innovative Primary System Configuration

In this section a possible alternate scheme of the reactor pool is presented that relies on a direct steam cycle produced by direct contact heat exchange between water and lead-bismuth. **Figure 20** illustrates a schematic of the proposed concept.

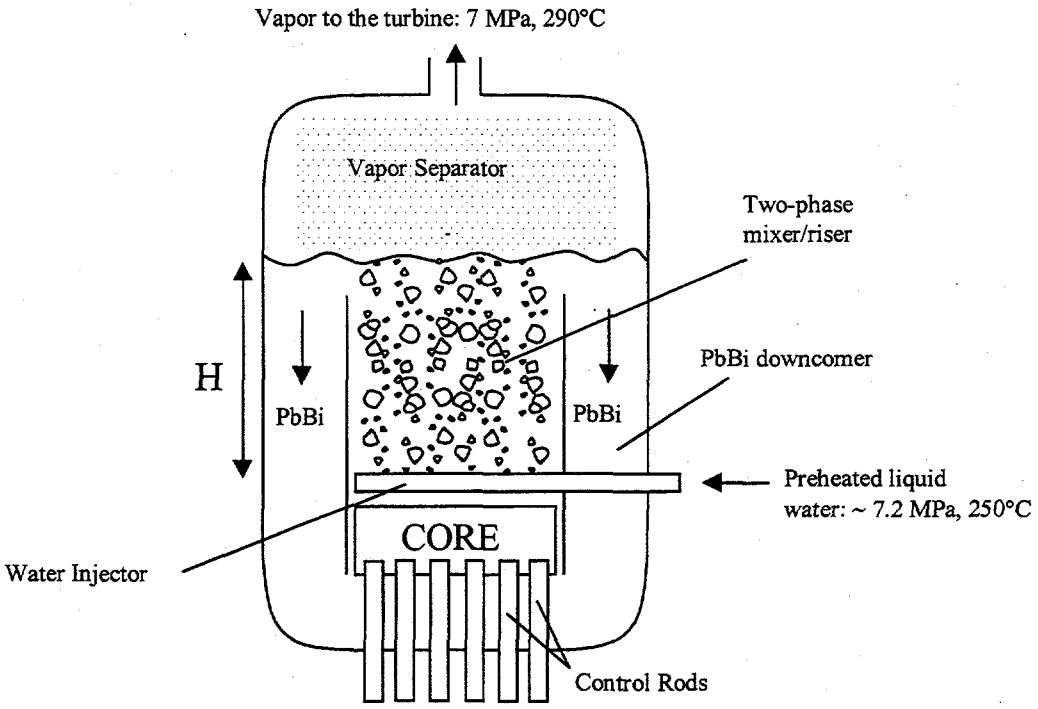

Figure 20. Direct steam cycle produced by injecting water into molten lead-bismuth.

Subcooled water is injected in the hot lead-bismuth above the core. The direct contact between the fluids causes water to rapidly vaporize leading to the formation of voids in the hot leg. The vapor is separated in the upper part of the reactor vessel and sent to the turbine. The large density difference between the cold and the hot leg drives the natural circulation of Pb-Bi in the vessel. The secondary coolant operates a Rankine cycle identical to a BWR that can achieve thermal efficiencies above 30%. The required vessel is within the design envelope of the ESBWR and operates at 290°C.

The direct heat transfer of Pb-Bi with water has been investigated in Israel for over a decade: an extensive experimental database [Branover, 1999] and the computational tools to predict the behavior of PbBi-water systems are available.

Some advantages of this innovative reactor design over the more traditional one introduced earlier are identified:

a) Preliminary calculations show that full power natural circulation (even at very low core p/d) can be easily achieved in this system with the following benefits:

   - A significantly shorter reactor pool (10 m vs. 20 m) can be designed. A shorter pool makes the reactor overall size smaller and requires a substantially lower inventory of Bi hence cutting the capital costs.

   - The maximum Pb-Bi temperature can be kept relatively low (<500°C vs. >550°C); see **Figure 21**.

   - An average Pb-Bi core velocity above 2 m/s is achieved, which enables removal of high linear heat generation rates in the fuel (see 3.4.2).

b) Elimination of the pumps and heat exchangers makes the operation more reliable.

c) Preliminary MCNP simulations indicate that the thermal-hydraulics of the two-phase hot leg and the core neutronics are decoupled, which may considerably decrease the concern of flow and neutronic instabilities.

d) Preliminary MCNP simulations indicate that accidental flooding of the core with liquid water does not cause reactivity to increase.

On the other hand new challenges arise:

a) The primary system needs to be pressurized, which increases its cost.

b) The consequences of mixing Pb-Bi and water in terms of chemistry control of the primary system are not clear.

c) A small Pb-Bi inventory may be undesirable if a large amount of decay heat is to be initially stored in the reactor pool upon loss of the normal heat sink (see 3.5.2).

d) The inclusion of separators into the primary vessel will complicate reactor refueling.

e) Direct contact of Pb-Bi and steam significantly aggravates the issue of polonium contamination.

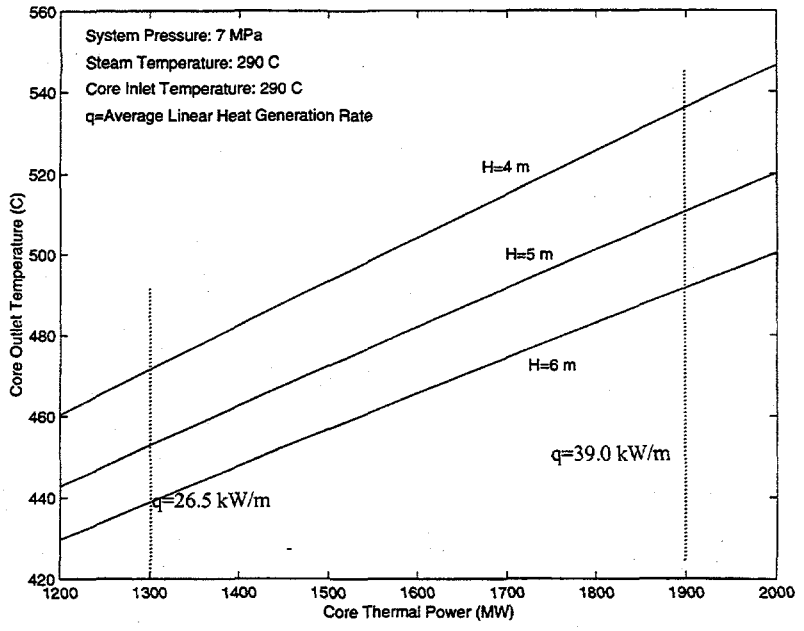

Figure 21. Core outlet temperature versus core power and gravitational head in a direct steam cycle reactor.

The latter problem is felt to be the most serious limitation of this design. The rate of formation and release of Po and its compounds (i.e. mainly PbPo and H_2Po) in steam is directly proportional to their concentration in the Pb-Bi coolant.

A first evaluation of the magnitude of Pb-Bi activation shows that the amount of Po in the reactor can be substantially reduced by continuous purification of a small fraction of the primary coolant inventory (see **Figure 22**). When created by neutron activation, polonium rapidly forms a stable compound with lead (i.e. PbPo). Upon contact of this compound with water a very volatile polonium hydride (i.e. H_2Po) is formed, which entrains steam hence contaminating it. A parallel mechanism of Po release into steam is direct evaporation of PbPo. The magnitude of Po release associated with both mechanisms will be assessed.

Some small leakages of contaminated steam out of the turbine are inevitable and will be a radioactive hazard. It must be demonstrated that the polonium concentration of the leaking steam is within prescribed limits (10 Bq/m^3).

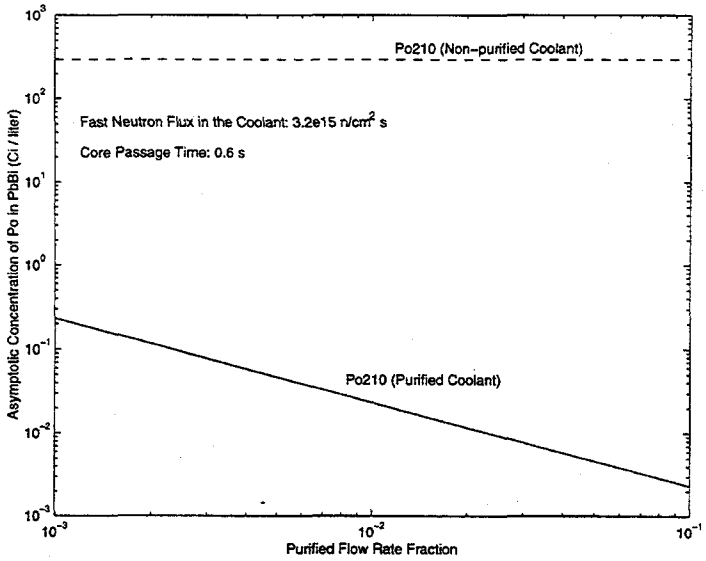

Figure 22. Concentration of polonium in the lead-bismuth coolant as a function of purification flow rate

3.6 Decay Heat Removal System (MIT)

3.6.1 Decay Heat after Shut-Down

Accurate knowledge of the decay power in the first few hours after shut down is essential to design the decay heat removal system (DHRS) and to predict the consequences of most accidents. In **Figure 23** the decay heat rate of the actinide-burning reactor (indicated as "trans") is compared to that of a typical PWR for several values of the burnup. As expected, the difference appears to be within the inherent uncertainties of the model used to calculate the decay power.

3.6.2 Steady-State Analysis

After the reactor has been shut down, the heat produced by the radioactive decay of the residual fission fragments poses a serious threat to the integrity of the nuclear fuel. Normally this heat is removed from the reactor pool through the primary-to-secondary-coolant heat exchanger, but means must be provided to ensure continuous cooling of the nuclear fuel should that heat removal path fail. To increase the reliability of the emergency decay heat removal, it is desirable to select a system that operates passively.

The heat can be removed by means of dedicated heat exchangers located in the reactor pool (as in most sodium cooled fast reactors) or it can be discharged to the environment through the reactor vessel.

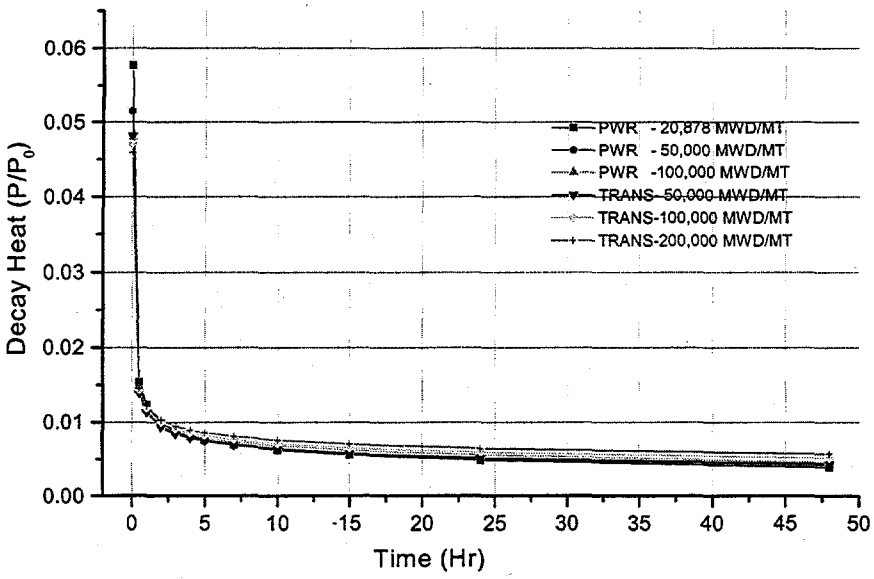

Figure 23. Comparison of of the decay heat in a pressurized water reactor at various burnup levels with the decay heat in an actinide-burning reactor.

Only the latter case has been so far investigated in this project. Two basic configurations are shown in **Figure 24** and were considered:

a) The decay heat is removed by natural circulation of air on the outer surface of the reactor containment.

b) The decay heat is removed by boiling water at the outer surface of the reactor containment.

Design a) is supported by the previous experience of the advanced sodium-cooled reactor project undertaken by GE [GE, 1991], to which we refer for its general technical characteristics. However, it should be noted that the GE system was conceived for a reactor of rather small power and some changes are then needed to make it suitable to our larger reactor design.

The heat produced in the core is conveyed by naturally circulating Pb-Bi to the surface of the reactor vessel. The gap between the vessel and the containment vessel can be filled either with an inert gas (e.g. nitrogen) or with a liquid metal (e.g. Pb-Bi or Pb). In the first case the heat is transferred through the gap mainly by radiation and large temperature gradients are expected. On the other hand, if a metal bond is employed, conduction and convection make the gap thermal resistance very small.

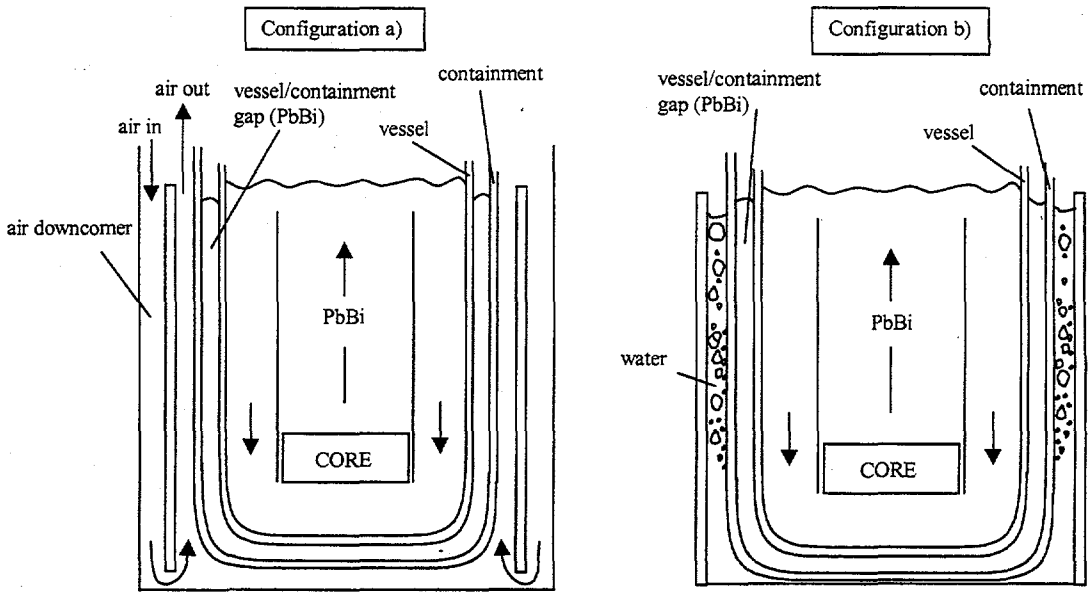

Figure 24. Reactor schematics for two approaches for removing decay heat; natural circulation of air on the outside surface and use of boiling water on the outside surface.

In configuration a) air enters the reactor building through two inlets and flows through the downcomer to the containment bottom. From here it flows upward in the riser where it is heated and it is finally discharged to the atmosphere through four stacks that supply the gravitation head needed to passively drive the air through the circuit[5].

In configuration b) the annular region around the containment is flooded with water. If the heat flux at the outer surface of the containment is large enough, boiling occurs and the produced vapor must be vented.

Tables 10 and 11 report the geometric characteristics of the vessel, the containment and the air system.

Table 10. Reactor Vessel and Containment

Vessel Outer Diameter (m)	6.0
Vessel Thickness (cm)	5.0
Vessel Height (m)	15
Vessel/Containment Gap (cm)	5
Containment Thickness (cm)	2.5

Table 11. Air System

Inlet Temperature (°C)	37
Stack Height (m)	30
Inlets	2
Outlets	4
Cold Air Tube Length (m)	30
Cold Air Tube Diameter (m)	2
Hot Air Tube Length (m)	40
Hot Air Tube Diameter (m)	3
Riser Thickness (cm)	12

[5] In Figure 24 the air inlets and exhaust stacks are not shown.

In **Figure 25** the performance of configurations a) and b) are compared for the case of vessel/containment gap filled with Pb-Bi. The primary coolant maximum temperature is plotted versus the decay power expressed as a fraction of the nominal thermal power of the core (assumed to be 1,800 MWthh).

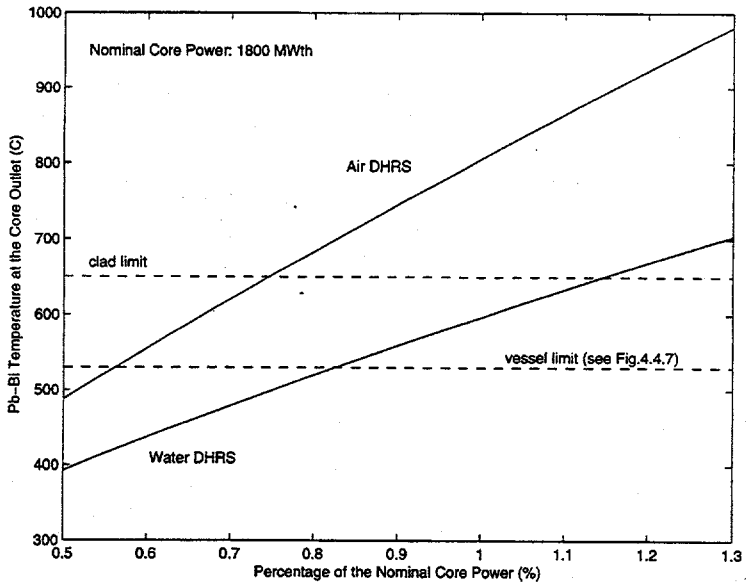

Figure 25. Maximum primary coolant temperature versus the decay power for two decay-heat-removal configurations.

As expected, the DHRS based on boiling water consistently provides better heat removal. The reactor vessel[6] temperature limits (see Section 3.5.4) are exceeded at 0.55% of the nominal core power for configuration a) and at 0.85% for configuration b). However, it can be shown that if the vessel/containment gap is filled with nitrogen, it is impossible to keep the Pb-Bi maximum temperature within acceptable limits at any power level of practical interest. Thus the vessel/containment gap must be filled with a thermal bond (i.e. Pb-Bi or Pb).

These results also show that, when the reactor is normally operating, it is possible to let the DHRS run without dissipating too high a power. In case of sudden loss of the normal heat sink, this ensures immediate removal of the decay heat and reduces the risk of the reactor coolant overheating. Nevertheless, it may prove preferable to operate with a dry containment vessel pit and only flood with water when the occasion demands.

[6] Here the vessel thickness is assumed to be 5 cm.

3.6.3 Reactor Pool Thermal Inertia

Depending on the primary system configuration the average Pb-Bi temperature under normal operating conditions can range between 300 to 400°C. Assuming an average Pb-Bi density of 10,200 kg/m^3 the coolant inventory in the reactor pool is approximately 3,030 tons. The coolant specific heat is 146.5 J/kg°C.

In Section 3.6.1 it was shown that the maximum decay power removable at steady state by the DHRS is approximately 15.3 MW (i.e. 0.85% of the nominal reactor power). It takes about 3.5 hours before the decay power falls to this level. Even though the DHRS is activated immediately, during this time the decay heat release rate is not matched by the rate of heat removal and the average temperature of the primary coolant in the reactor pool increases hence reaching a maximum at 3.5 hrs after shutdown. It is important to ensure that this maximum temperature does not exceed the vessel temperature limit (i.e. ~ 525°C for a 5-cm thick vessel). An energy balance over the reactor pool shows that the Pb-Bi temperature rise at 3.5 hrs is approximately 125°C, hence leading to a maximum temperature of 525°C.

On the other hand, if the DHRS activation is not instantaneous (e.g. DHRS is activated 3.5 hours after shutdown), all the decay heat is accumulated in the primary coolant causing a clearly unacceptable temperature rise of about 635°C !

One way to reduce this figure is to fill the vessel/containment gap with solid Pb and to allow it to melt when the reactor is shut down hence absorbing a significant fraction of the decay energy released in the core. Assuming even a 30 cm vessel/containment gap entirely filled with pure solid lead, the primary coolant temperature rise after 3.5 hrs is approximately 445°C, which is still too high.

Therefore it seems crucial to guarantee that the DHRS can be activated almost immediately after shut down (i.e. within few minutes). In this case 15.3 MW are constantly removed and it appears to be possible to maintain the primary coolant temperature within acceptable limits.

3.7 Power Cycle (MIT)

3.7.1 Temperature Constraints

The thermal efficiency of the power cycle strongly depends on the temperature at which the heat is supplied by the primary to the secondary coolant. It is clear that in principle a high cycle maximum temperature is desirable. In practice the mechanical and corrosion characteristics of the core, vessel and heat exchanger materials set the limit (see Section **3.3**). The interim selected cladding material (i.e. the Russian steel EP-823) exhibits acceptable corrosion resistance to the lead-bismuth eutectic for temperatures up to 650°C[7]. If a typical 100°C temperature drop across the Pb-Bi boundary layer is

[7] However, the mechanical strength of this material rapidly decreases with temperature above 500°C.

assumed (see Section **3.3**), the primary coolant bulk temperature limit is around 550°C. Assuming a further 50°C temperature drop across the heat exchanger, the maximum temperature achievable in the power cycle seems to be approximately 500°C.

Also the choice of the secondary coolant temperature at the inlet of the heat exchanger requires some attention. It must be sufficiently above 125°C (i.e. the freezing point of Pb-Bi at atmospheric pressure) to provide margin to undesirable freezing of the primary coolant during transients. At the same time, it must be smaller than the minimum Pb-Bi temperature in the primary system (which in turn is determined by natural circulation requirements, see Section **3.4**). In practice, the available design window for this temperature is 125 to 250°C, which requires preheating of the working fluid: this is done by means of the regenerator in a gas cycle and by means of the feedwater heaters in a steam cycle.

Finally the cycle minimum temperature is limited by the conditions of the ultimate heat sink (i.e. typically seawater or air at 20 to 30°C).

3.7.2 Gas Turbine Cycle

Gas cycles are generally simpler, more compact than steam cycles and offer potential for more automated operation. In our case helium is chosen as the working fluid for its chemical inertness and its relatively high thermal conductivity. However, while significant experience has been accumulated on air gas turbine cycles, only little relatively has been accumulated on helium cycles.

Figure 26 illustrates the schematic and the T-s diagram of the Brayton cycle of choice. Regenerative heat transfer between the turbine outlet stream and the high pressure compressor outlet stream increases the cycle thermal efficiency and helps achieve higher temperatures at the inlet of the PbBi/He heat exchanger hence complying with the requirement discussed in **Section 3.7.1**. The use of inter-cooling increases the net work per unit mass and widens the regeneration temperature window. An alternate configuration with two inter-coolers is also explored.

Re-heating of the hot helium was discarded to keep the design of the PbBi/He HX simple.

The turbine and compressor efficiencies and the regenerator effectiveness are assumed to be 92, 92 and 65%, respectively. The cycle minimum temperature is set equal to 50°C. The cycle maximum pressure is set equal to 7.0 MPa. Several values of the cycle compression ratio are explored with the goal of maximizing the thermal efficiency.

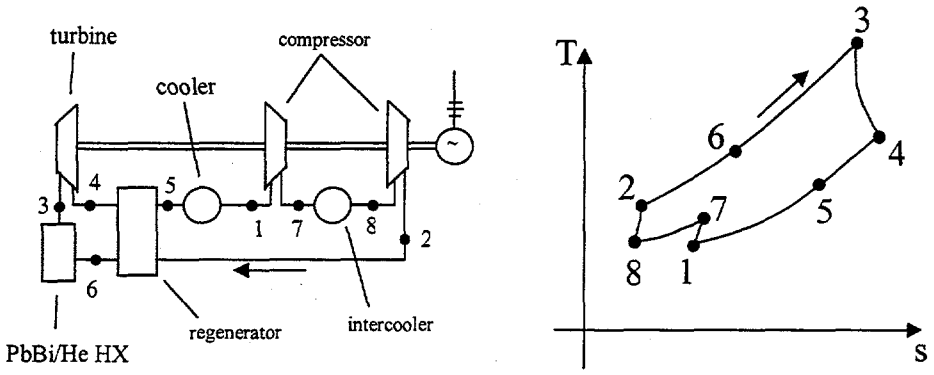

Figure 26. Brayton cycle temperature versus enthalpy diagram.

Figure 27 illustrates the thermal efficiency as a function of the compression ratio for the configuration with one and two inter-coolers and for a 500°C cycle maximum temperature. The net work per unit mass ranges from 300 to 450 kJ/kg. Values of T_6 (i.e. the heat exchanger inlet temperature) are within the required 125 to 250°C range. It should be noted that the addition of a second inter-cooler significantly improves the thermal efficiency, which, however, remains below 30%.

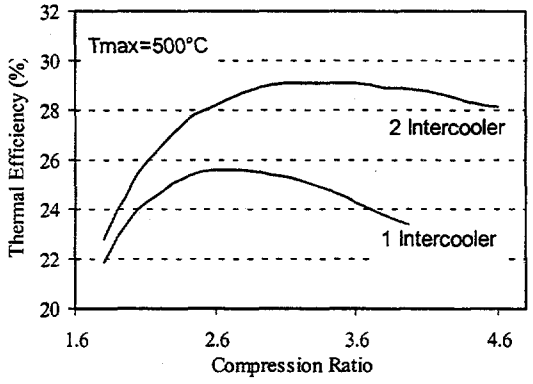

Figure 27. Thermal efficiency as a function of compression ratio.

Values of the thermal efficiency comparable to current LWR plants (~33%) may be achieved at the expense of cycle complexity and cost by adding a third inter-cooler and/or by re-heating the turbine outlet stream helium and/or by increasing the regenerator size and hence its effectivness.

A reference design of the PbBi/He HX was established with the following characteristics:

- Exchanged power: 1,800 MWth
- Counter-flow shell-and-tubes: PbBi in the shell/He in the tubes
- 180,000 circular smooth tubes made of EP-823 stainless steel; OD 8 mm; wall thickness 1 mm; length 6 m
- Triangular lattice (p/d=1.45)
- PbBi inlet/outlet temperature: 250°C/550°C
- He inlet/outlet temperature: 200°C/500°C

The heat exchanger occupies the entire annular region between the core barrel and the reactor vessel (see **Figure 13**)

3.7.3 Steam Cycle

The steam turbine option has not been thoroughly investigated so far; thus we limit this section to some preliminary considerations.

The characteristics that make water an attractive secondary coolant are:

a) its low cost,
b) the long and successful experience with operating steam cycle power plants,
c) the possibility of achieving relatively high thermal efficiency (>30%) at low maximum temperature (<400°C),
d) the possibility of designing a compact PbBi/water HX due to the high heat transfer coefficient of boiling water.

On the other hand:

a) water is corrosive and requires careful chemistry control,
b) Rankine cycles are generally rather complicated and costly.

If an indirect scheme is chosen (see section 3.5.1), it is possible to employ a supercritical Rankine cycle (i.e. a cycle operating above the critical pressure of water) and to obtain thermal efficiencies as high as 42% [Adamov et al. 1992].

If a direct scheme is chosen (see Section 3.5.6), the limit on the operating pressure is set by the design of the reactor vessel. The BWR experience indicates that:

a) a large vessel at approximately 7.0 MPa can be designed and safely operated,
b) thermal efficiencies above 30% can be achieved if saturated steam at 7.0 MPa is produced.

3.8 Development of a RELAP5 Version for Lead-Bismuth Cooled Reactors (INEEL)

The RELAP5 computer code (LMITCO 1995) was developed to calculate the thermal-hydraulic response of nuclear reactors and related experimental systems during various transients, such as loss of forced flow, loss of heat sink, and loss of coolant. The code models the hydraulic response of the working fluid, including both single- and two-phase effects, and the thermal response of heat structures such as fuel pins and steam generator tubes. Core power is calculated with a reactor kinetics model that accounts for thermal-hydraulic feedback and decay heat. The code is extremely flexible, allowing it to simulate a wide range of thermal-hydraulic systems. Although RELAP5 was primarily developed for analysis of commercial, light water reactors, it has been applied and assessed extensively for a variety of reactor designs.

The ATHENA computer program (Carlson et al. 1986) is based on RELAP5. ATHENA shares a common source code with RELAP5, but includes extensions to allow the use of other working fluids, including liquid metals, but not the lead-bismuth eutectic. Thus, the fluid properties of the lead-bismuth eutectic were added to ATHENA so that it could be used as a tool in the analysis of lead-bismuth reactor designs. The development of lead-bismuth fluid properties is described in Section 3.8.1.

Since the ATHENA code is based on RELAP5, which was primarily developed for analysis of light water reactors, it is appropriate to question the applicability of the code for analysis of lead-bismuth reactors. An evaluation of the applicability of the code for analysis of lead-bismuth reactors is presented in Section 3.8.2.

3.8.1 Lead-Bismuth Fluid Properties

The equation of state for the lead-bismuth eutectic was developed (Shieh 1999) as follows. First, the specific heats for both lead and bismuth up to the melting point of the alloy were obtained from standard tables. The specific heat of the alloy was computed as a weighted average of the lead and bismuth values according to their mass fractions (Young 1999). A simple integration technique was then used to find the enthalpy of the alloy in the solid state up to the melting point. This was then added to the latent heat of fusion data (Young 1999) to obtain the enthalpy of the liquid alloy at the melting point. The density and temperature at the melting point were also obtained from the tables.

A soft sphere model (Young 1977) was then used to find the equation of state of the alloy. The soft sphere model is based on the generalized Van der Waal's equation that has five adjustable parameters. Two of these parameters plus two constants used in the model are the same for both lead and bismuth and therefore the same for the alloy. The procedure to find the remaining three parameters is to solve the two simultaneous nonlinear equations, i.e.

Pressure at the melting point = 0, and

Energy at the melting point = enthalpy at melt.

These two equations were successfully solved for the three parameters using a standard numerical technique. Details of this procedure are given in the Software Design and Implementation Document (Shieh 1999).

ATHENA uses a simplified Clausis-Clapeyron formulation for the saturation pressure, P_{sat}:

$$P_{sat} = ce^{\gamma T}$$

where T is the temperature and c and γ are constants that were obtained from a least-squares curve fit of data (Nesmeyanov 1963).

ATHENA also requires equations for the transport properties of dynamic viscosity, thermal conductivity, and surface tension. These equations are described below. The dynamic viscosity, μ, is calculated as:

$$\mu = \psi \rho$$

where ψ is the kinematic viscosity and ρ is the density. The kinematic viscosity and density have been correlated (Touloukian et al. 1970) as:

$$\psi \ (m^2/s) = 61.423 \ (T - 273.15)^{-0.61106} * 10^{-7}$$
$$\rho \ (kg/m^3) = 10728.0 - 1.2159 \ (T - 273.15)$$

where T is the temperature in degrees K. The thermal conductivity, k, is calculated as a piecewise linear function (Touloukian et al. 1970):

$$k \ (W/m\text{-}K) = 9.408 - 0.00318 \ (T - 437.321) \text{ if } T < 437.321 \text{ K}$$
$$= 9.78 + 0.00973 \ (T - 475.554) \text{ if } 437.321 \text{ K} < T < 475.554 \text{ K}$$
$$= 9.78 + 0.0131 \ (T - 475.554) \text{ if } T > 475.554 \text{ K}$$

The surface tension, σ, is calculated based on data (Lyon 1952) as:

$$\sigma \ (N/m) = -5.5 \times 10^{-5} \ (T - 1073.15) + 0.367$$

3.8.2 Code Applicability Evaluation

Because of its high boiling point, the lead-bismuth eutectic will be a single-phase liquid during normal reactor operation and most transients. This greatly simplifies the applicability evaluation since ATHENA's two-phase models, which constitute much of the coding, are relatively unimportant. The most important phenomena that the code needs to be able to model for lead-bismuth are heat transfer and wall friction.

ATHENA contains many heat transfer correlations to simulate several heat transfer regimes, including forced and natural convection, nucleate boiling, critical heat flux, transition boiling, film boiling, and condensation. However, forced convection is the only regime expected to occur with lead-bismuth. For lead-bismuth and other liquid metals, the code calculates the forced convection Nusselt number, Nu, as:

$$Nu = 5 + 0.025\ Pe^{0.8}$$

where Pe is the Peclet number. This correlation is applicable for fully developed flow of a liquid metal in a tube with constant wall temperature (Bird et al. 1960). A separate correlation for natural convection is not required because the Nusselt number approaches five, rather than zero, as the Reynolds number goes to zero.

ATHENA allows the user to apply correlations developed for rod bundles rather than tubes for specific heat structures. However, this option was not available for liquid metals in the original code. Thus, a correlation developed by Westinghouse for rod bundles (Todreas and Kazimi 1990) was added to the code. The correlation is:

$$Nu = 4.0 + 0.33(P/D)^{3.8}(Pe/100)^{0.86} + 0.16(P/D)^{5}$$

where P/D is the pitch-to-diameter ratio of the rods. The correlation was developed for a range of $1.1 < P/D < 1.4$ and $10 < Pe < 5000$.

ATHENA calculates single-phase wall friction using the Darcy-Weisbach friction factor for laminar and turbulent flow. Turbulent flow is of most interest for lead-bismuth reactors. For turbulent flow, the code uses the Zigrang-Sylvester approximation (Zigrang and Sylvester 1985) to the Colebrook-White correlation (Colebrook 1939) to compute the friction factor. The Zigrang-Sylvester approximation is accurate to within 0.5% of the Colebrook-White correlation (LMITCO 1995). The SSC code (Guppy et al. 1983), which was developed for analysis of liquid metal fast breeder reactors, used an explicit approximation to the Colebrook-White correlation that was accurate to within 5%. The Colebrook-White correlation also is in good agreement with a correlation used in previous analyses (Greenspan et al. 1998) of lead cooled reactors. Thus, it is judged that the code's model is applicable for the calculation of single-phase wall friction in lead-bismuth reactors.

Phenomena that are not important in water, and thus were justifiably neglected in RELAP5, could be more important in liquid metals. Two such phenomena, axial heat conduction in the fluid and thermal entry length, were evaluated to determine their potential importance in a lead-bismuth reactor.

The thermal-conductivity in lead-bismuth is more than an order of magnitude greater than that of water. Thus, axial conduction within the fluid has the potential to be more important in lead-bismuth than in water. Axial conduction effects can generally be neglected if the Peclet number is greater than 100 (Kays and Crawford 1980). At normal operation, the core and steam generator tube design described in Section 3.9 have Peclet

numbers greater than 3000. The effects of axial conduction could begin to be become significant only at very low flow rates, such as might occur during natural circulation. The Peclet number will be checked after transients involving natural circulation are simulated. Until then, it seems appropriate to neglect axial conduction.

The forced convection heat transfer correlations used by the code for lead-bismuth are based on fully developed flow. The thermal entry length depends on the Prandtl number, and is longer for fluids with low Prandtl number fluids, such as liquid metals, than for water. Based on results for a circular tube with constant heat flux (Kays and Crawford 1980), the average heat transfer coefficient over the length of the core described in Section 3.9.1 during full-power operation is about 25% greater than the fully developed heat transfer coefficient. The average heat transfer coefficient for the steam generator tubes described in Section 3.9.2 is less than 10% greater than the fully developed value. Since the code does not model thermal entry effects, it is expected to provide somewhat conservative calculations of fuel temperature and heat exchanger efficiency.

ATHENA has a fundamental limitation for cases in which water enters the reactor system, such as would occur in the direct steam cycle described in Section 3.4.5 or in the case of a steam generator tube rupture. The limitation arises because the code solves continuity, energy, and momentum equations for two phases of a single fluid, lead-bismuth in this case. If water enters the system, four phases will be present: liquid lead-bismuth, a tiny amount of lead-bismuth vapor, liquid water, and steam. The code cannot handle this situation mechanistically as it represents only two fluid fields, one for the liquid and one for the gas. A major revision to the code would be required to model all four phases and the interactions between them. However, since the liquid water will boil to steam, acceptable results can probably be obtained by representing the steam as an ideal, non-condensable gas. A control system would be required to inject an appropriate amount of non-condensable gas and to remove from the lead-bismuth coolant the amount of energy needed to boil the water to steam.

The addition of water into the primary coolant will result in a two-phase flow. The predicted void fraction in the two-phase region will be governed by the code's bubble size and interphase drag correlations. These correlations are important because they will affect the natural circulation flow rate and determine whether or not steam flows into the core, where any voiding may significantly affect the reactivity. The applicability of these correlations for a lead-bismuth reactor has not yet been evaluated but has been deferred until the need arises.

In summary, the evaluation indicates that the ATHENA code is generally applicable for analysis of lead-bismuth reactors. The important code models of single-phase forced convection heat transfer and wall friction were judged to be applicable. The code will predict average heat transfer coefficients that are up to 25% lower than would be expected in the reactor because it assumes fully developed flow. The neglected effects of axial conduction were judged to be not important. The code cannot mechanistically represent the effects of adding water into the reactor coolant, but it is believed that the most important of these effects can be modeled adequately for design calculations. The

applicability of the code's interphase drag correlations for lead-bismuth/steam mixtures will be determined as the need arises.

3.9 Lead-Bismuth Cooled Reactor Thermal-Hydraulic Design (INEEL)

The INEEL design of the lead-bismuth-cooled reactor is based on the design illustrated in **Figure 13**. The primary differences between this design and the one described in Section 3.5 are that the heat exchangers are steam generators, with water on the shell side, and reactor coolant pumps are located in the downcomer below the steam generators to provide forced circulation. Details of the core and steam generator designs are provided in Sections 3.9.1 and 3.9.2, respectively. Note that the thermal-hydraulic design has not been optimized and thus is considered preliminary.

3.9.1 Core Design

The basic core design is consistent with the one analyzed in Section 3.2 and is summarized in **Table 12**. The core lattice is relatively open with a pitch-to-diameter ratio of 1.6. The large pitch-to-diameter ratio was chosen to reduce the frictional pressure drop across the core and thus enhance natural circulation, while still providing acceptable neutronic characteristics. The lattice is square, which results in a subchannel that is bounded by four adjacent fuel rods. The flow area fraction within each subchannel is 0.69, with the remainder of the area occupied by the fuel rods. When this fraction is applied to the entire area within the core barrel, the flow area is approximately 6.7 m^2, which is the value currently assumed in the analysis.

Russian experience (MacDonald 1999) with lead-bismuth indicates that the oxygen content of the fluid must be tightly controlled to prevent slag formation and that hydrogen will have to be added to the system periodically to breakdown the slag. The fluid velocity must be at least 1 m/s to properly distribute the hydrogen. However, erosion problems can occur if the fluid velocity exceeds 3 m/s. The design fluid velocity in the core was chosen to be at an intermediate value, 2 m/s, to avoid these problems.

Table 12. Core design.

Parameter	Value
Fuel pellet outer diameter	8.64 mm
Fuel composition (wt%)	20% of Pu+actinides, 80% of Zr
Gap thickness (at BOL)	0.2 mm
Bond material - lead-bismuth-tin alloy (wt%)	33%Pb-33%Sn-33%Bi
Cladding thickness	0.63 mm
Composition of cladding material	SS 304
Fuel pin outer diameter	10.3 mm
Pitch	16.48 mm
Pitch to diameter	1.6
Heated core length	1.2 m
Gas plenum height	0.9 m
Core barrel inner diameter	3.5 m
Pool vessel inner diameter	5.0 m
Core power	1000 MW_t
Fluid velocity	2.0 m/s

3.9.2 Steam Generator Design

Four basic criteria were used in the evaluation of steam generator designs. First, the designs evaluated were similar to those of commercial pressurized water reactors (PWRs) to reduce development costs. Second, the lead-bismuth fluid velocity was selected to be 2 m/s for the reasons described in the previous section. Third, the lead-bismuth was assumed on the tube side and the water on the shell side. This arrangement was selected to minimize potential problems with materials. However, it is recognized that reversing the arrangement and placing the lead-bismuth on the shell side would reduce the frictional pressure drop through the tubes by about 40%, thus enhancing natural circulation. Finally, the length of the steam generator tubes was selected so that the exit temperature of the lead-bismuth would be within about 5 C of the saturation temperature on the secondary side. In commercial PWRs, the cold leg temperature is generally about 10 C higher than the saturation temperature on the secondary side.

Three separate steam generator designs have been considered. The first design was a vertical once-through steam generator (once through steam generator) similar to a Babcock and Wilcox PWR. This steam generator contains an annular downcomer region that is separated from the boiler region, which contains the tubes, by a thin shell. Feedwater enters the downcomer, flows downwards and enters the bottom of the boiler, which contains the tubes. The flow is upwards through the boiler which is counter to the downwards flow of lead-bismuth inside the tubes. As the water flows up the boiler, it is heated until reaching dry superheated steam, which then flows into the steam lines.

The second design is a horizontal steam generator similar to those used in Russian VVERs except that the tubes are once through rather than bent. In this design, the tubes are in the lower half of the steam generator vessel and the mixture level is maintained

above the top row of tubes. Due to the large flow area and relatively small velocities, the steam rises to the top of the horizontal vessel and the liquid naturally separates due to the effects of gravity. Dryers can be added to the top of the steam generator if necessary.

A vertical U-tube design was considered briefly, but this design was dropped because the tube length required to cool the lead-bismuth to within 5 C of the secondary saturation temperature was less than the length of an average 180° U-bend.

The first two steam generator designs are summarized in **Table 13**. The values in the table are for a single steam generator. Four steam generators are required to remove the core power. The steam generator tube lengths are much shorter than in commercial PWRs, but the vessel diameters are comparable. The vessel diameters are too large to allow the steam generators to fit into the annular gap between the core barrel and the pool vessel (see **Table 12**). Consequently, the steam generators can not be immersed in the pool unless the pool vessel inner diameter is increased significantly.

Table 13. Steam generator designs.

Parameter	Vertical once through steam generator	Horizontal once through steam generator
Lattice	Triangular	Triangular
Number of tubes	13,255	13,288
Tube outer diameter	0.0147 m	0.0147 m
Tube thickness	0.001 m	0.001 m
Tube length	3.8 m	2.8 m
Pitch to diameter	1.5	1.5
Secondary hydraulic diameter	0.022 m	0.022 m
Vessel inner diameter	2.85	3.8

The following section compares the two steam generators during full-power operation.

3.10 System Modeling Studies (INEEL)

An ATHENA model of the lead-bismuth cooled reactor system has been developed. The system model uses the horizontal once through steam generator described in Section 3.9.2. A stand-alone model of the vertical once through steam generator described in Section 3.9.2. has also been developed. Both input models are described in Section 3.10.1. Steady-state results obtained with both models are described in Section 3.10.2.

3.10.1 Input Models

The ATHENA model of the lead-bismuth cooled reactor system is shown in **Figure 28**. The model represents the lead-bismuth pool as two regions that are separated by the core barrel. The region inside the core barrel, which contains the core and upper plenum, is represented with Components 510 and 520. The upper pool region, which is located

above the core barrel, is modeled with Components 530, 535, and 540. The liquid level normally resides in Component 535. Component 540 contains a cover gas at near atmospheric pressure that sets the pressure of the system. The region outside the core barrel contains the steam generators, reactor coolant pumps, and down-comer. In the design, the down-comer is separated into four quadrants, each connected to one steam generator and reactor coolant pump. For simplicity, the four steam generators, pumps,

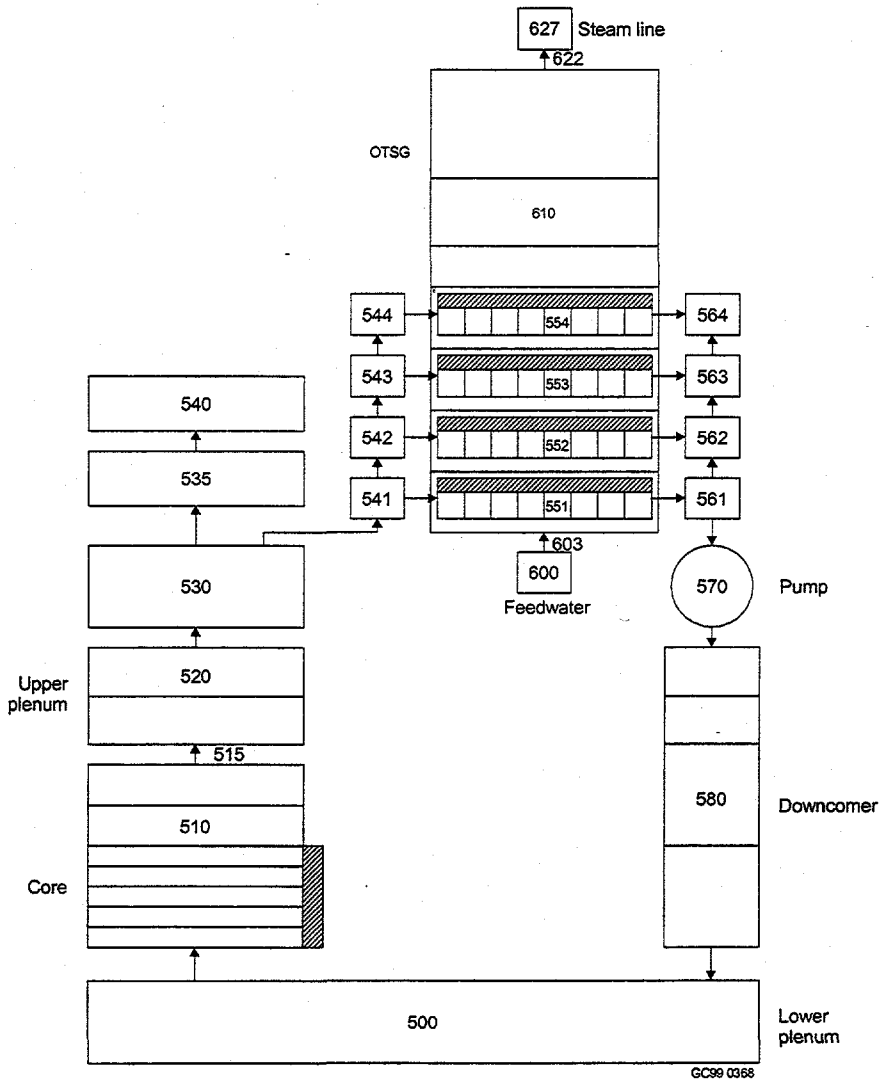

Figure 28. ATHENA system model.

and down-comer quadrants are combined into a single flow path in the model. As the design matures, it is relatively simple to expand the model so that it represents each quadrant separately. Component 500 represents the lower plenum region, which connects the down-comer and core.

The horizontal once through steam generator is represented as an inlet plenum (Components 541 through 544), steam generator tubes (Components 551 through 554), and outlet plenum (Components 561 through 564). The steam generator is divided into four layers of tubes so that the effects of a decreasing secondary liquid level in loss-of-heat sink events can be simulated. The lowest layer contains approximately 10% of the tubes while each of the other layers contains about 30%.

The secondary side of the steam generator is modeled in two halves. The lower half contains the tubes and is divided into four levels consistent with the primary side nodalization. The upper half is divided into three levels to allow separation of steam. Boundary conditions are used to set the feedwater flow rate and steam line pressure. The steam line pressure was set at 6.89 MPa, which is representative of the secondary pressure in commercial PWRs.

The bottom of the steam generator tubes is currently about 4 m above the top of the active core. However, this distance may be changed to improve the performance of the system during transients.

The ATHENA system model contains 67 volumes and 69 junctions.

The stand-alone model of the vertical once through steam generator is shown in **Figure 29**. The primary side of the tubes is represented with Component 550. Normally flow is down through the tubes. The secondary side of the steam generator is modeled with three components representing the downcomer (Component 605), boiler (Component 610), and upper annulus (Component 615) regions. Boundary conditions are used to set the hot leg temperature, cold leg pressure, and flow rate on the primary side and the feedwater flow rate and steam line pressure on the secondary side.

3.10.2 Steady-State Results

The ATHENA system model with the horizontal once through steam generator was used to perform a full-power, steady state calculation. The results of the steady-state calculation are summarized in **Table 14**.

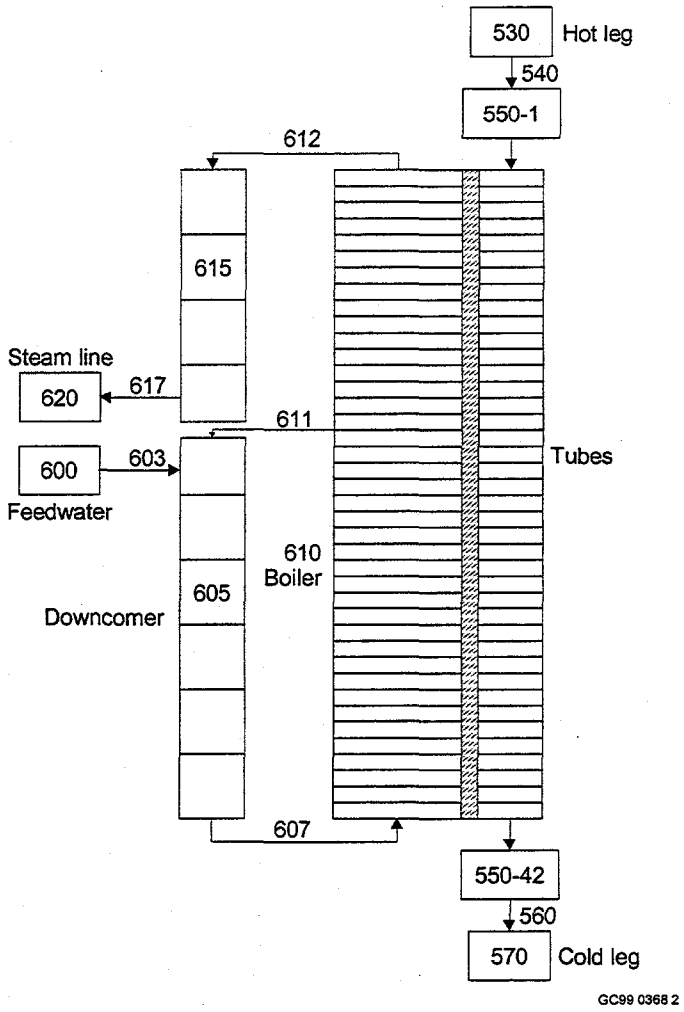

Figure 29. ATHENA model of the vertical once through steam generator.

Table 14. Steady-state results with the ATHENA system model.

Parameter	Value
Core power	1000 MW_t
Lead-bismuth flow rate	1.38×10^5 kg/s
Hot leg temperature	340.9 C
Cold leg temperature	292.8 C
Secondary fluid temperature	284.8 C
Core fluid velocity	2.0 m/s
Once through steam generator tube velocity	2.0 m/s
Pump differential pressure	140 kPa
Lead-bismuth fluid mass	2.1×10^6 kg

The core fluid velocity was chosen to be 2.0 m/s to avoid materials problems as described in Section 3.9.1. Choosing the fluid velocity essentially determines the system mass flow rate since the core flow area is known from the geometry and the density of the lead-bismuth is only a weak function of temperature. The additional specification of the core power then determines the fluid temperature rise across the core. The cold leg temperature is governed by the secondary temperature, which is set by the assumed steam line pressure, and the length of the steam generator tubes. The resulting cold leg temperature of the current design is similar to those of commercial PWRs. Coincidentally, the temperature rise across the core is also quite similar to commercial PWRs.

The pressure rise generated by the pump for this design is about 25% of that in commercial PWRs. Assuming the same pump efficiency, the ratio of pump power to core power in this design is only about half that of existing PWRs. Thus, the pumping power requirements for this design should be acceptable. About 60% of the pressure rise across the pump is dissipated in the once through steam generator tubes and most of the remainder is dissipated in the core.

The temperature difference between the upper plenum and downcomer generates a gravitational head that is about 3% of that produced by the pump. The temperature rise across the core during natural circulation should be less than that shown in **Table 12** once the core power drops to 3%. Thus, the design is expected to have adequate natural circulation characteristics. The natural circulation flow rate in this design is much less than the 100% value for the design described in Section 3.5.1. The primary reasons for the different natural circulation flow rates are that the temperature rise is much smaller in this design (48 C versus 300 C), the fluid velocity is between 2 and 4 times higher, and the lead-bismuth is assumed to be inside rather than outside of the tubes.

A steady-state calculation using the vertical once through steam generator model was also performed. **Table 15** presents a comparison of the results with the horizontal and vertical once through steam generator models. The values shown represent the total of four steam generators.

Table 15. Steam generator results.

Parameter	**Horizontal once through steam generator**	**Vertical once through steam generator**
Power, MW_t	1002	994
Secondary pressure, MPa	6.89	6.89
Feedwater flow rate, kg/s	611	552
Feedwater temperature, K	533	533
Steam temperature, K	558	597
Collapsed liquid level, m	1.10	1.57
Total fluid mass, kg	18,600	20,800

The power removed by the horizontal once through steam generator is the total of the core power and the pump heat. The power removed by the vertical once through steam

generator is about 1% too low and can be increased by adding more feedwater. One of the most significant differences between steam generators is that the vertical once through steam generator produces steam that is 39 C superheated whereas the horizontal once through steam generator produces saturated steam. Consequently, the vertical once through steam generator will be more efficient. However, the vertical once through steam generator also requires a longer tube because of the poorer heat transfer characteristics in the post-dryout regimes. The longer tube causes an increase in the frictional pressure drop and poorer natural circulation characteristics.

One of the advantages of both steam generators compared to the lead-bismuth-helium heat exchangers described in Section 3.7.2 is that the initial inventory of water can be used to remove core decay heat and lessen the demands on the DHRS. For example, the amount of liquid initially present in the horizontal once through steam generator can remove at least 7 minutes of decay power before drying out. It would be relatively easy to increase the initial liquid level in the horizontal once through steam generator and thus provide more decay heat removal capability. For example, the steam generators in some PWRs are able to remove decay heat for more than an hour after a total loss of feedwater. Similar results should be possible with this design.

4. MAJOR TECHNICAL ACCOMPLISHMENTS

4.1 Neutronics

A reference core geometry and fuel composition were established that:

- yield negative reactivity feedback upon total or partial coolant voiding, and
- provide enough excess reactivity for the non-fertile fuel at BOL to operate on an 18 month refueling cycle.

B_4C was chosen as the control material.

Preliminary data on reactivity and fuel life for fertile fuel was obtained, with the fuel choice being a Pu-Th-Zr (+depleted U).

4.2 Materials

The fuel thermal conductivity variation with temperature and burnup was calculated based on models developed by ANL for the IFR metallic fuel.

4.3 Plant Engineering

A design envelope was established for the following items:

- full power natural circulation in the primary system;
- linear power limits in the fuel;
- vessel temperature limits;
- decay heat removal system; and
- gas turbine power cycle.

The following tasks were performed to develop a system analysis capability:

- lead-bismuth fluid properties were added to a version of the ATHENA code;
- the ATHENA code was shown to be generally applicable for the analysis of lead-bismuth cooled reactors;
- ATHENA models of preliminary designs were created; and
- the ATHENA models were used to perform steady-state calculations at full power.

5. MAJOR REMAINING TECHNICAL CHALLENGES AND FUTURE WORK

5.1 Neutronics

(a) Verify the core reactivity stability throughout the burnup cycle.
(b) Achieve a suitable doppler feedback.
(c) Reduce the axial power peaking due to control rod insertion.
(d) Investigate the implications of the two different approaches to actinide burning (i.e. critical reactor vs. ATW) in terms of neutronic safety and fuel cycle.
(e) Achieve a core lifetime of ~15 years for fertile fuel.
(f) Keep the U-233 <12wt% of the total uranium content for fertile fuel, while maintaining core life and non-proliferation concerns.
(g) Keep the power density less than that of Na cooled reactors (~80%).
(h) Do an economic comparison of non-fertile and fertile fuel cycles.

5.1.1 Planned Papers and Conferences for Neutronics Work

Listed are currently proposed papers/conferences and submittal dates for the work that has been done.

- "Computational Results of Metallic and Nitride Fuels for Advanced Lead-Bismuth Cooled Fast Reactors", *Eighth International Conference On Nuclear Engineering* – ICONE-8. Abstract to be submitted September 15, 1999.
- "Comparative Study of Reactivity Trends of Lead/Lead-Bismuth Cooled Small Long-Life Nuclear Reactors". Manuscript to be submitted to *Nuclear Technology*, September 30, 1999.
- "Design Criteria and Computational Results for Optimal Fuel Composition of a Long Life Lead-Bismuth Cooled Nuclear Reactor". Manuscript to be submitted to *Nuclear Engineering Design*, October 30, 1999.

Other papers/conferences will be submitted as work progresses. These will include, but are not limited to, optimal core designs, safety and non-proliferation issues, and economic estimation/analysis/comparison of lead-bismuth cooled reactors.

5.2 Materials

(a) Advance the knowledge and understanding of Pb-Bi interaction with reactor materials with the goal of accurately establishing the temperature limits.

(b) Select a set of suitable materials for the fuel cladding, the gap thermal bond, the core internals and the reactor vessel.

Los Alamos National Laboratory (LANL) has already acquired some information on the Russian experience with Pb-Bi: an effort will be made to bring this knowledge to the INEEL and MIT.

The possibility of setting up an experimental Pb-Bi loop at MIT and/or the INEEL will be considered with the following goals:

- validate the Russian approach to the corrosion issue,
- explore alternative approaches,
- establish a US Pb-Bi database.

5.3 Plant Engineering

(a) Establish in quantitative terms the trade-off between natural circulation capability, reactor size, reactor power and costs.
(b) Explore innovative primary system configurations.
(c) Assess the economic and technical impact of the polonium issue.
(d) Select a suitable power conversion cycle.

No matter what primary system configuration is selected, the problem of managing the coolant activation to form Po will be a key question. Information on the chemical characteristics of Polonium and its compounds is rare and incomplete. MIT will evaluate the possibility of undertaking an experimental program with the goal of assessing:

- the basic thermodynamic properties of Po and its compounds;
- a suitable way to separate Po from Pb-Bi; and
- rate of release of Po and its compounds in air and water.

The technical challenges related to the development of system analysis capability and future work are:

- develop ATHENA input for reactor kinetics to simulate feedback between the thermal-hydraulics and neutronics;
- develop models of the DHRS; and
- simulate various transients, such as loss of flow and loss of heat sink, to investigate the safety characteristics of the design.

5.3.1 Planned Papers and Conferences for Plant Engineering Work (INEEL)

Two papers are tentatively planned for submittal to a journal or conference. The topics for these papers include the addition of lead-bismuth fluid properties into the ATHENA code and the simulation of various transients to investigate the safety characteristics of the design.

6. REFERENCES

Adamov, E., et al. 1997. "The next generation of fast reactors". *Nuclear Engineering and Design*, Vol.173, p.143.

Asher, R. C., D. Davies and S. A. Beetham 1977. Some observations on the Compatibility of Structural Materials with Molten Lead, *Corrosion Science*, Volume 17, No. 7, Pergamon Press, pp. 545-557.

Bauer, T.H., 1993. "A general analytical approach toward the thermal conductivity of porous media". *Int. J. Heat Mass. Transfer*, Vol. 36, No. 17, pp. 4181-4191.

Bauer, T.H., et al. 1993. "In-pile measurement of the thermal conductivity of irradiated metallic fuel". *Nuclear Technology*, Vol. 110, pp. 407-421.

Bird, R. B., W. E. Stewart, E. N. Lightfoot, 1960. *Transport Phenomena*, John Wiley & Sons, Inc., New York.

Bichuya, A. L., 1969. Effect of Oxide Films on the Corrosion-Fatigue Strength of 1Cr18Ni9Ti Steel in Liquid Pb-Bi Eutectic, *Soviet Materials Science*, July-August 1969, pp. 352-354.

Branover, H., et al. 1999. "Heavy-liquid-metal two-phase flow with steam". *Transactions of the 1999 ANS Annual Meeting. Boston*, June.
Branover, H., et al. 1994. Some Problems of the Corrosion and Protection of Materials in Liquid Metal MHD Generators, *Journal of Material Letters 13*, Chapman & Hall, pp. 508-511.

Carlson, K. E. et al., 1986. *ATHENA Code Manual Vol. I: Code Structure, System Models, and Solution Methods*, EGG-RTH-7397, September.

Cathcart, J. V., and W. D. Manly 1954. A Technique for Corrosion Testing in Liquid Lead, ORNL-1737, Oak Ridge National Laboratory, August.

Chitaykin, V. I., 1999. Status of ATW Technology and Research Needs from the Perspective of MINATOM, presented at the ATW Workshop, Washington, D. C., February 16-18, 1998.

Colebrook, C. F., 1939. "Turbulent Flow in Pipes with Particular Reference to the Transition Region Between Smooth and Rough Pipe Laws", *Journal of Institute of Civil Engineers*, 11, pp. 133-156.

DeHoff, R. T. 1993. *Thermodynamics in Materials Science,* McGraw-Hill, pp. 499-504.

GE Nuclear Energy, 1991. *ALMR Summary Plant Design Description.*

Greenspan, E., E. Elias, W. E. Kastenberg, and N. Stone, 1998. *Non-Proliferating Liquid Metal Cooled Reactors for Developing Countries*, University of California at Berkeley, CNTWM98-2, February 15, 1998.

Guppy, J. G. et al., 1983. Super System Code (SSC, Rev. 0), *An Advanced Thermohydraulic Simulation Code for Transients in LMFBRs*, NUREG/CR-3169, BNL-NUREG-51650, April.

Hill R.N., et al. 1989. "Physics Studies of Weapons Plutonium Disposition in the Integral Fast Reactor Closed Fuel Cycle". *Nucl. Sci. Eng.*, Vol. 121, pp. 17-31.

Horsley, G. W., and J. T. Maskrey 1958. The Corrosion of 2 % Cr-1% Mo Steel by Liquid Bismuth, *Journal of The Iron and Steel Institute*, June, pp. 139-148.

Kays, W. M. and M. E. Crawford, 1980. *Convective Heat and Mass Transfer, Second Edition*, McGraw-Hill Book Company.

Kazimi, M.S., and M.D.Carelli, 1976. *Heat transfer correlation for analysis of CRBRP assemblies*. Westinghouse Report, CRBRP-ARD-0034. The essential results are also reported in N.E.Todreas and M.S.Kazimi, *Nuclear Systems I*, 10, p.451. Taylor&Francis, 1990.

LMITCO, 1995. *RELAP5/MOD3 Code Manual*, NUREG/CR-5535, INEL-95/0174, Volumes 1 through 7, August.

Lyon, R. N., 1952. *Liquid Metals Handbook*, Navy Press.

MacDonald, P. E., 1999. Personal communication, March.

Manly, W. D. 1958. *Fundamentals of Liquid Metal Corrosion*, ORNL-2055, Oak Ridge National Laboratory.

Nesmeyanov, A. N., 1963. *Vapor Pressure of the Chemical Elements*, Elsevier Publishing Co.,

Sekimoto, H., Su'ud, Z., 1994. "Design Study of Lead and Lead-Bismuth-Cooled Small Long-Life Nuclear Power Reactors Using Metallic and Nitride Fuel", *Nuclear Technology*, 109, 1995, pp. 307-313.

Shieh, A., 1999. "Addition of Lead-Bismuth Eutectic as a Working Fluid in the ATHENA Code", LMITCO, to be published.

Su'ud, Z., Sekimoto, H., 1995. "Design and Safety Aspect of Lead and Lead-Bismuth Cooled Long-Life Small Safe Fast Reactors for Various Core Configurations", *Journal of Nuclear Science and Technology*, 32, 1995, pp. 8-19.

Taylor, J. W., 1956. Inhibition of Liquid-Metal Corrosion, U. S. Atomic Energy Commission Report AERE-M/TN-35 [Great Britain Atomic Energy Research Establishment, Harwell, Berkshire, England].

Todreas, N. E. and M. S. Kazimi, 1990. *Nuclear Systems I, Thermal Hydraulic Fundamentals*, Taylor and Frances.

Touloukian et al., 1970. *Thermophysical Properties of Matter: Thermal Conductivity of Metallic Liquids*, IFI/Plenum, New York.

Tsirlin, M., et al. 1998. On Some Aspects of Structural Materials Compatibility with Liquid Lead-Containing Coolants.

F.Venneri ,1998. "Notes on the LANL ATW project". Presentation held at MIT, January.

Vreeland, D. C., et al. 1953. Corrosion Tests for Liquid Metals, Fused Salts at High Temperatues, Nucleonics, November, pp. 36-39.

Weeks, J. R., and C. J. Klamut 1960. Reactions Between Steel Surfaces and Zirconium in Liquid Bismuth, *Nuclear Science and Engineering*, 8, pp. 133-147.

Weeks, J. R., and A. J. Romano 1969. Liquidus Curves and Corrosion of Fe, Ti, Zr. And Cu in Liquid Bi-Pb Alloys, *Corrosion-NACE*, Vol. 25, No. 3, pp. 131-136.

Young, D. A., 1977. *A Soft Sphere Model for Liquid Metals*, Lawrence Livermore Laboratory, UCRL 52352.

Young, D. A., 1999. Private communications with A. Shieh.

Zigrang, D. J. and N. D. Sylvester, 1985. "A Review of Explicit Friction Factor Equations", *Transactions of ASME, Journal of Energy Resources Technology*, 107, 1985, pp. 280-283.